Journal Pre-proof

Design, Synthesis, Biological Activity Evaluation of 3-(4-Phenyl-1H-Imidazol-2-yl)-1H-Pyrazole Derivatives as Potent JAK 2/3 and Aurora A/B Kinases Multi-targeted Inhibitors

You-Guang Zheng, Jin-An Wang, Long Meng, Xin Pei, Ling Zhang, Lin An, Cheng-Lin Li, Ying-Long Miao

PII: S0223-5234(20)30906-5

DOI: https://doi.org/10.1016/j.ejmech.2020.112934

Reference: EJMECH 112934

To appear in: *European Journal of Medicinal Chemistry*

Received Date: 21 August 2020

Revised Date: 6 October 2020

Accepted Date: 9 October 2020

Please cite this article as: Y.-G. Zheng, J.-A. Wang, L. Meng, X. Pei, L. Zhang, L. An, C.-L. Li, Y.-L. Miao, Design, Synthesis, Biological Activity Evaluation of 3-(4-Phenyl-1H-Imidazol-2-yl)-1H-Pyrazole Derivatives as Potent JAK 2/3 and Aurora A/B Kinases Multi-targeted Inhibitors, *European Journal of Medicinal Chemistry*, https://doi.org/10.1016/j.ejmech.2020.112934.

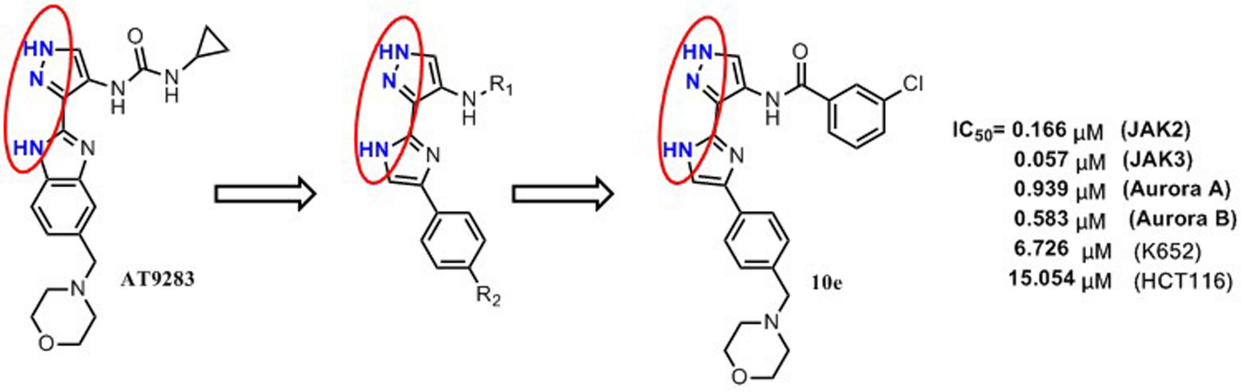

18Design, Synthesis, Biological Activity Evaluation of 3-(4-Phenyl-1H-Imidazol-2-yl)-1H-Pyrazole Derivatives as Potent JAK 2/3 and Aurora A/B Kinases Multi-targeted Inhibitors

You-Guang Zheng[a, b*], Jin-An Wang[c], Long Meng[a, b], Xin Pei[a, b], Ling Zhang[a, b], Lin An[a, b], Cheng-Lin Li[a, b], Ying-Long Miao[c].

[a]College of Pharmacy, Xuzhou Medical University, Xuzhou 221004, PR China;

[b]Jiangsu Key Laboratory of New Drug Research and Clinical Pharmacy, Xuzhou Medical University, Xuzhou 221004, PR China;

[c] Center for Computational Biology and Department of Molecular Biosciences, University of Kansas, Lawrence, KS 66047, USA.

Youguang Zheng, Jin-An Wang and Long Meng contributed equally to this work.

ABSTRACT

In this study, a series of 3-(4-phenyl-1H-imidazol-2-yl)-1H-pyrazole derivatives were designed, synthesized, and evaluated for their biological activities. Upon performing kinase assays, most of the compounds exhibited potent inhibition against JAK2/3 and Aurora A/B with the IC_{50} values ranging from 0.008 to 2.52 μM. Among these derivatives, compound **10e** expressed the most moderate inhibiting activities against all the four kinases with the IC_{50} values of 0.166 μM (JAK2), 0.057 μM (JAK3), 0.939 μM (Aurora A), and 0.583 μM (Aurora B), respectively. Moreover, most of the derived compounds exhibited potent cytotoxicity against human chronic myeloid leukemia cells K562 and human colon cancer cells HCT116, while compound **10e** expressed antiproliferative activities against K562 (IC_{50} = 6.726μM). According to western blot analysis, compound **10e** down-regulated the phosphorylation of STAT3, STAT5, Aurora A, and Aurora B in a dose-dependent manner in K562 and HCT116 cells. Cell cycle analysis revealed that compound **10e** inhibited the proliferation of cells by inducing cell cycle arrest in the G2 phase. The molecular modeling suggested that compound **10e** could maintain a binding mode similar to the binding mode of AT9832, a common JAK 2/3 and Aurora A/B kinases multi-target kinase inhibitor. Therefore, compound **10e** might be a potential agent for cancer therapy deserving further research.

Keywords: JAK2/3, Aurora kinases, pyrazole derivatives, multi-targeted inhibitors

1. Introduction

The Janus kinases (JAKs) family, consisting of four structurally related kinases, JAK1, JAK2, JAK3, and TYK2, regulates the JAK/STAT signaling pathway [1, 2]. The JAK/STAT pathway plays a vital role in the oncogenesis in the immune system [3], and mediates signaling by cytokines, which control survival, proliferation, and differentiation of several cell types, such as human chronic myeloid leukemia K562 cells [4-6], human colorectal cancer HCT-116 cells [7-9] and other cancer cells [10-14]. In recent years, the JAK kinase inhibitors that target the JAK/STAT pathway, such as Ruxolitinib, has been approved by FDA [15], extensively studied [16-18] and provided a great value for the treatment of myeloproliferative neoplasias and beyond [19]. In addition, some JAK inhibitors have been developed and introduced into clinical trials, such as AZD1480 [20], Fedratinib [21], AT9283 [22] and so on (Fig.1).

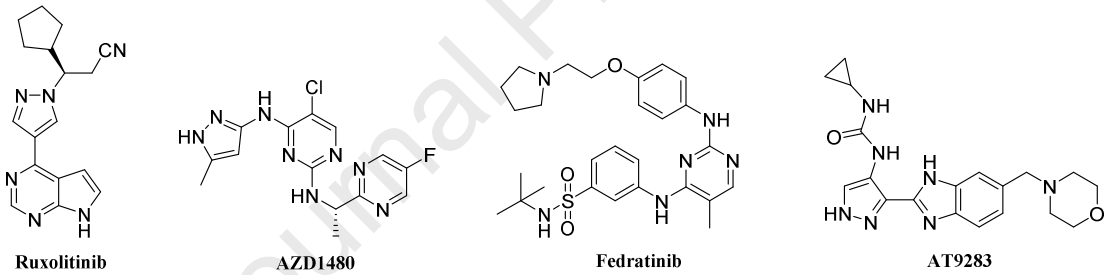

Fig.1 Chemical structures of JAK inhibitors.

Aurora kinases belong to serine/threonine kinases that are involved in chromosome condensation, spindle dynamics, kinetochore-microtubule interactions, chromosome orientation, and establishment of the metaphase plate during mitosis [23]. The family includes three kinases designated as Aurora A, B, and C, which possess a very similar sequence, particularly in the carboxy-terminal catalytic domain [24]. Overexpression of aurora kinases in several human tumors has made them appealing targets for the development of anticancer therapies [23-26]. Over the past decades, some Aurora kinase inhibitors have been developed for the treatment of cancer, such as VX-680 [27], AT9283 [22], CYC-116 [28], AZD-1152 [29], AMG-900 [30], PHA-739358 [31], MLN8054 [32], MLN8237 [33] and ENMD2076 [34] (Fig.2).

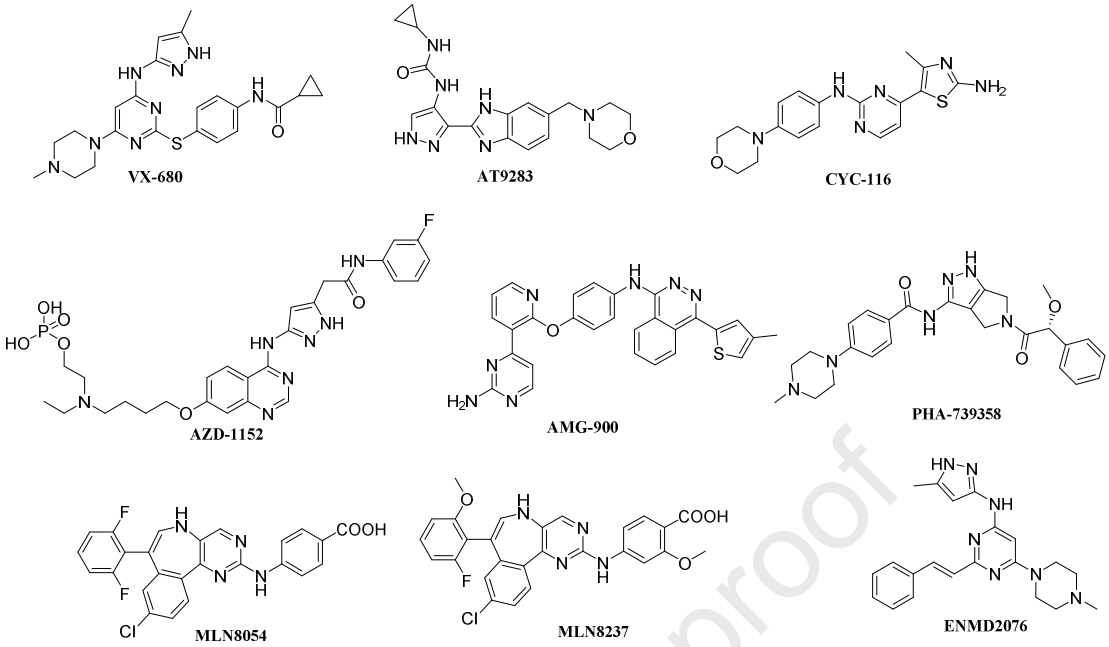

Fig.2 Chemical structures of Aurora inhibitors

Although recent studies have identified a significant number of single-targeted selective kinase inhibitors and proven their efficacy in treatment for specific cancers [35-37], the mortality rate caused by cancer remains high. Therefore, the multi-targeted kinase inhibitors could exhibit more potent therapeutic effects by synergistic effects as well as by the combination of various antitumor mechanisms [38]. Meanwhile, studies have also confirmed that the Aurora kinase and JAKs multi-target inhibitors can inhibit the growth of tumor cells more effectively than the selective aurora kinase inhibitors [39]. AT9283 is a multi-target kinase inhibitor, which can effectively inhibit the activities of Aurora A, Aurora B, JAK2, JAK3, and ABL1 kinases [40]. According to the reported crystal structure study, AT9283 complexed with Aurora-A by forming hydrogen-bonds to the backbone carbonyl groups of Glu211, as well as to the backbone NH and carbonyl groups of Ala213 of the protein hinge region [40].

In this paper, retaining the hydrogen-bonded pharmacophore of AT9283, a series of 3-(4-phenyl-1H-imidazol-2-yl)-1H-pyrazole derivatives were rationally designed and synthesized as JAK 2/3 and Aurora A/B kinases multi-target inhibitors.

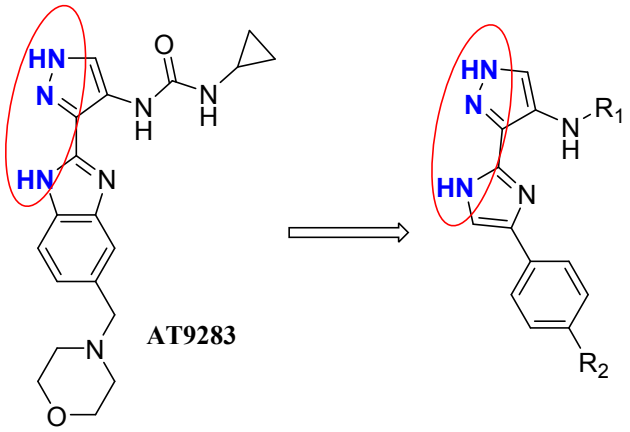

Fig.3 Design of novel s3-(4-phenyl-1H-imidazol-2-yl)-1H-pyrazole derivatives

2. Results and discussion

2.1. Chemistry

As depicted in Scheme 1, *N*-protection of 4-nitropyrazol-3-carboxylic acid (**1**) was performed by treating with DHP reagent to obtain compound (**2**). Compound **(6)** was synthesized from compound **(3)** by bromomethylation and *N*-alkylation, followed by bromination of ketones at α-position. Compound **(2)** reacted with compound (**6**) to produce compound (**7**), which was treated with ammonium acetate and acetic acid to afford compound (**8**). Then after, compounds (**8**) were reduced to its amino derivatives (**9**) using H_2, and Pd/C. The target compounds (**10**) were prepared by reacting compound (**9**) with various benzoic acids or chloropyrimidines.

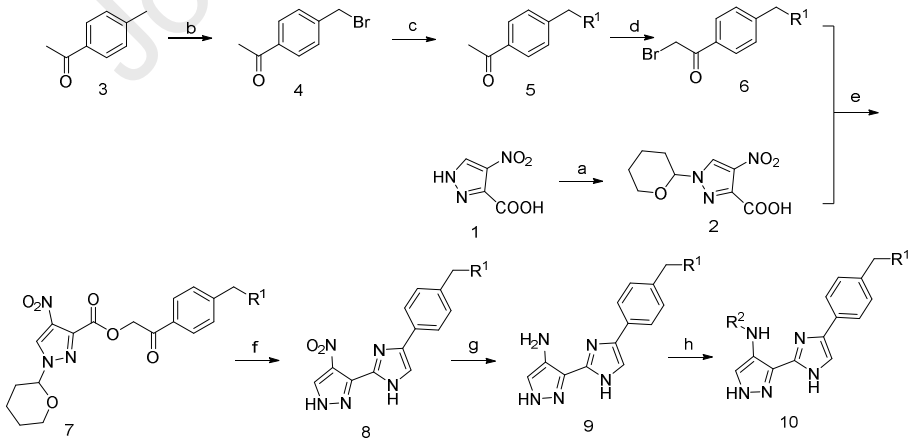

Scheme 1. The synthesis of compounds **10a-10j**. Reagents and conditions: (a) DHP, PTSA, THF; (b) NBS, AIBN, Acetonitrile; (c) K_2CO_3, KI, Acetonitrile; (d) Br_2, CH_3COOH, HBr; (e) K_2CO_3, KI, Acetonitrile; (f) CH_3COONH_4, CH_3COOH, Reflux; (g) H_2, Pd/C, CH_3OH; (h) standard amide and aminopyrimidine coupling methods (for specific reagents, see the experimental section)

The overall synthetic route of compounds **18a** starting from 4-hydroxyacetophenone (**11**), has been outlined in Scheme 2. Compounds (**17**) were obtained upon sequential

O-alkylation, *N*-alkylation, bromination of ketones at α position, followed by esterification, cyclization, and reduction. Further, the target compounds (**18a**) were prepared by treating compound (**17**) with different chloropyrimidines.

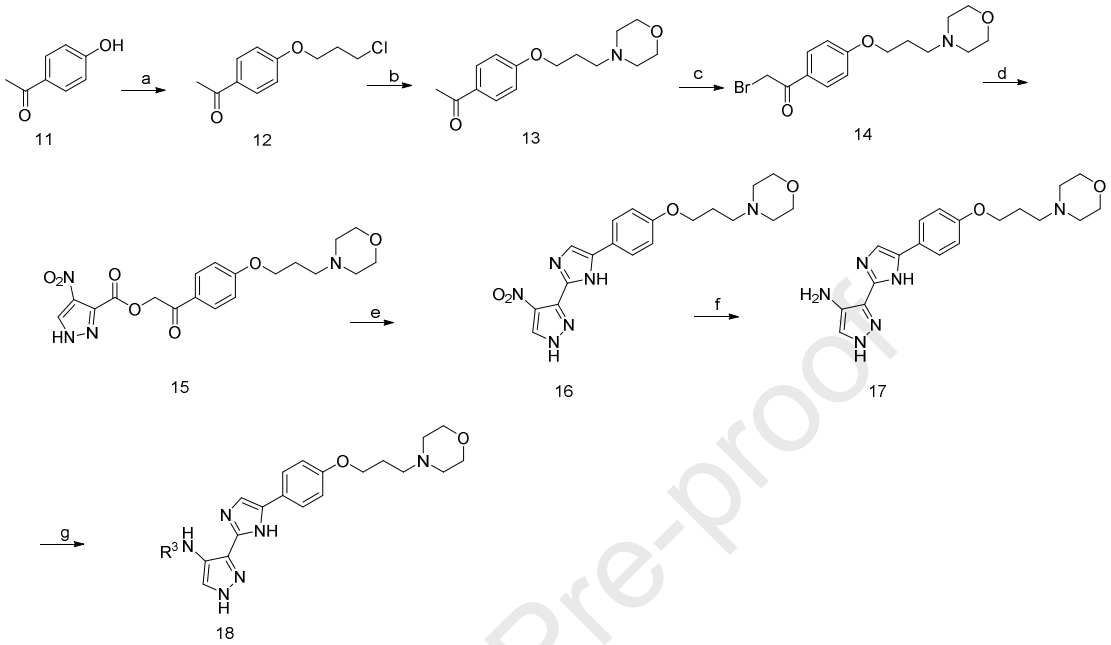

Scheme 2. The synthesis of compounds **18a**. Reagents and conditions: (a) Trimethylene chlorobromide, K_2CO_3, KI, Acetonitrile; (b)Morpholine, K_2CO_3, KI, Acetonitrile; (c) Br_2, CH_3COOH, HBr; (d) Compound **2**, K_2CO_3, KI, Acetonitrile; (e) CH_3COONH_4, CH_3COOH, Reflux; (f) H_2, Pd/C, CH_3OH; (g) Chlor pyrimidine, NaI, DIPEA, DMF.

2.2. Biological activities

The target compounds were evaluated for their enzymatic activities against Aurora A, Aurora B, JAK2, and JAK3. Additionally, the *in vitro* antiproliferative effects of the targeted compounds against human chronic myeloid leukemia cells K562 and human colon cancer cells HCT116 were also carried out. The results were summarized in Table 1.

2.2.1. *In vitro* inhibition activities studies of kinases

As shown in Table 1, most of the compounds (**10a-10j**) exhibited potent inhibition against JAK2/3 and Aurora A/B with the IC_{50} values ranging from 0.008 to 2.52 μM. Among these derivatives, compound **10e** expressed the most moderate inhibiting activities against all the four kinases with the IC_{50} values, 0.166 μM (JAK2), 0.057 μM (JAK3), 0.939 μM (Aurora A), and 0.583 μM (Aurora B), respectively. Compounds (**10b**, **10d**, **10e**, and **10i**) containing –Cl and–OCH_3 groups at the benzene

ring of R^2 exhibited selective inhibiting activities against JAKs (approximately 20-fold selectivity), while compound **10c** bearing a nitro group at the benzene ring of R^2 showed pan-inhibiting activities against JAK2/3 and Aurora A/B. In addition, replacement of the benzoyl group of R^2 with a pyrimidine group (compound **10j**) increased the inhibition activities against JAK2/3 and Aurora A (JAK2 IC_{50} = 0.008μM, JAK3 IC_{50} = 0.023μM, and Aurora A IC_{50} = 0.145μM).

Table 1 Enzymatic activities and *In vitro* anti-proliferative activities in tumor cell lines of compounds **10a-10j**.

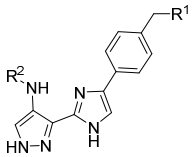

10

Compd	R^1	R^2	IC_{50}(μM)					
			JAK2	JAK3	Aurora A	Aurora B	K562	HCT116
10a		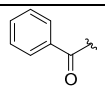	NT	NT	NT	NT	>10	>10
10b		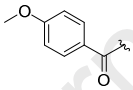	0.014	0.024	0.359	>1	5.652	>10
10c		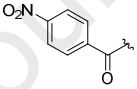	1.178	0.569	0.466	0.65	4.34	5.21
10d		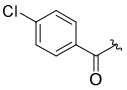	0.094	0.064	2.514	NT	2.63	>10
10e		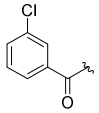	0.166	0.057	0.939	0.583	6.726	15.054
10f		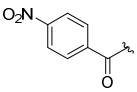	NT	NT	NT	NT	NT	NT
10g		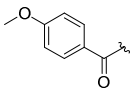	NT	NT	1.523	NT	>10	>10
10h		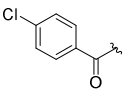	NT	NT	2.055	NT	>10	1.592

10i		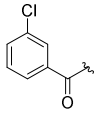	0.016	0.013	1.132	NT	2.503	>10
10j		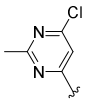	0.008	0.023	0.145	NT	10.048	>10
AT9283			0.0022	0.0012	0.026	0.062	0.748	0.09

NT (Not Test)

2.2.2. Antiproliferation assay

Most of our target compounds were tested against human chronic myeloid leukemia cell lines (K562) and human colorectal cancer cell line (HCT116), in which overexpression of JAKs and Aurora kinases remains prominent [40-43]. The results of the antiproliferative activities are shown in Table 1 and Table 2. Most compounds exhibit potent cytotoxicity against both of these tumor cell lines. In K562 cell lines, compounds **10b-10e** (IC_{50} values of 2.630–6.726 μM) having the morpholine ring at the side chain shown more potent antiproliferation activity in comparison to the compounds (**10 g** and **10 h**) with piperidine ring (IC_{50} values >10 μM). It was noted, compounds having –Cl, $–OCH_3$, and$–NO_2$ groups at the benzene ring (**10b-10e**) exhibited significant improvement to their proliferative inhibition; compound **10c** and **10d** that contained electron-withdrawing groups (Cl and NO_2) expressed slightly higher K562 proliferative inhibition (the IC_{50} = 4.34 μM, 2.63 μM, respectively) compare to **10b** having an electron-donating group (CH_3O-).

We also synthesized one compound bearing longer side chain at 4-position of the benzene ring (**18a**). As indicated in Table 2, Extension of the side chain (compound **18a**) displayed no significant change to cytotoxicity against K562 and HCT116.

Compound **10e**, which expressed the most potent inhibition on kinases and cancer cells, was selected for further study.

Table 2 Enzymatic activities and *In vitro* anti-proliferative activities in tumor cell lines of compounds **18a**.

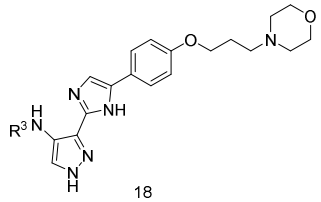

18

Compd	R^3	IC_{50}(μM)					
		JAK2	JAK3	Aurora A	Aurora B	K562	HCT116
18a	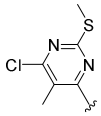	NT	NT	NT	NT	9.88	16.14
AT9283		0.0022	0.0012	0.026	0.062	0.748	0.09

NT (Not Test)

In addition, *in vitro* anti-proliferative activities of compound **10e** against human normal colon epithelial cells (HCoEpiC) and human umbilical vein endothelial cells (HUVEC) had been tested (Table 3). The result showed that **10e** has significantly lower toxic effect on HCoEpiC (IC_{50}=31.509μM) and HUVEC (IC_{50}=28.978μM) than AT9283 (IC_{50}=2.367μM, 1.793μM, respectively).

Table 3 *In vitro* anti-proliferative activities of compound **10e** against normal cells

	(IC_{50} μM)	
Compound	HCoEpiC	HUVEC
10e	31.509	28.978
AT9283	2.367	1.793

2.2.3 Compound **10e** blocks JAKs and Aurora kinases phosphorylation in K562 and HCT116 cell

Western blot analysis was performed to evaluate the performance of compound **10e** in a cellular context according to the published research works [44-47]. The phosphorylation of Aurora A, Aurora B, STAT3, and STAT5 was investigated in K562 and HCT116 cells by treating with various concentrations of compound **10e** (control, 1, 10, and 20 μM). The results demonstrated that multi-target kinase inhibitor **10e** also led to decreased levels of p-STAT3 and STAT5, which could be correlated with JAKs inhibition, indicating the inhibition of intracellular JAK-STATs

pathway. Furthermore, compound **10e** down-regulated the phosphorylation of Aurora A and Aurora B in a dose-dependent manner in K562 and HCT116 cells, respectively (Fig. 4). According to the above results, compound **10e** could be considered as a potential JAKs and Aurora kinases inhibitor.

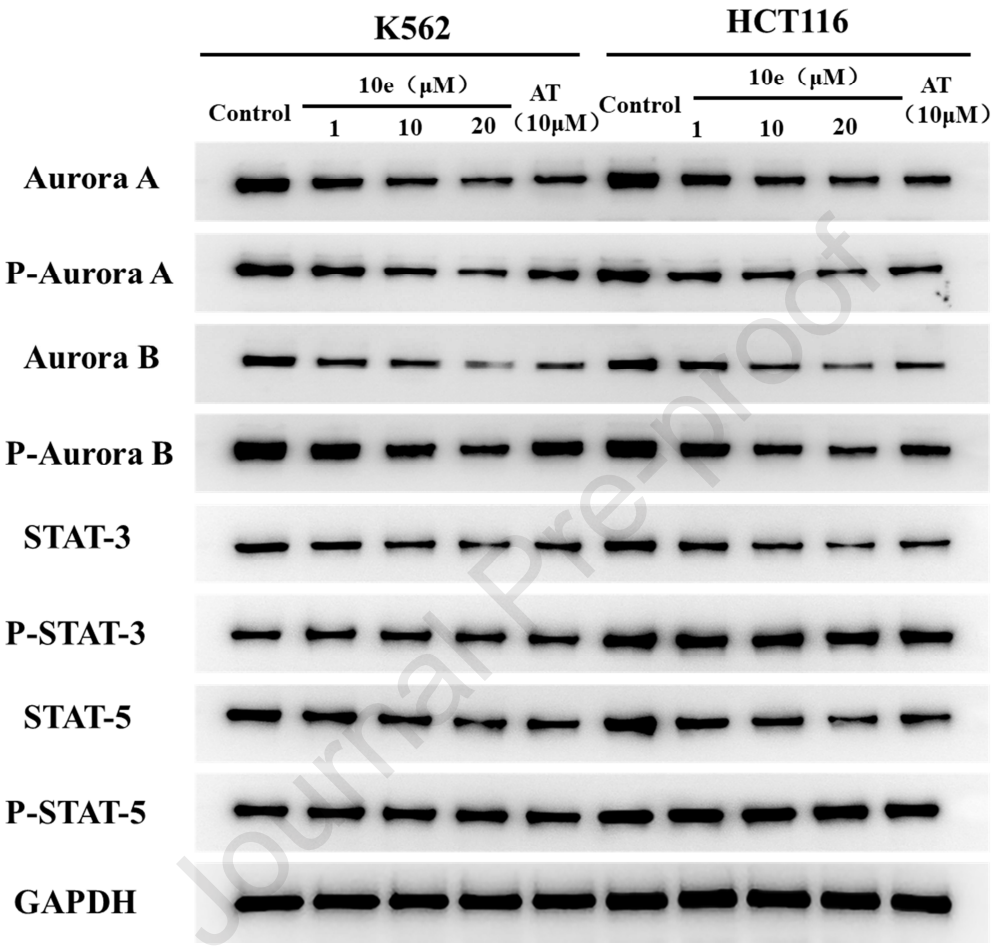

Fig. 4 Western blot analysis of p-Aurora A, p-Aurora B, p-STAT3 and p-STAT5 with various concentrations of compound **10e** in K562 and HCT116 cells. GAPDH was used as a loading control.

2.2.4 Cell cycle arrest

As per the previous reports, the JAK-STATs pathway and Aurora kinases could play important roles in controlling cell cycle progression [48, 49]. AT9283, which is a multi-target kinase inhibitor, induces common cancer cell-cycle arrest at the G2 phase [50, 51]. Accordingly, we tested the effects of **10e** on cell-cycle progression in K562 and HCT116 cells using flow cytometry. As shown in Fig. 5, a dose-dependent G2 phase transition arrest was observed in K562 and HCT116 cells when treated with **10e**.

Exposure of compound **10e** in K562 cell at 10 μM concentration resulted in 16.27% of cell arrest at the G2 phase, compared with 7.73% in untreated cultures and 14.99% in AT9283 (10 μM) treated cultures (Fig. 5A). On the other hand, exposure of compound **10e** in HCT116 cells at 10 μM resulted in 16.16% of cell arrest at the G2 phase, while the values for cell arrest in untreated cultures and in AT9283 (10 μM) treated cultures were 10.46% and 25.19%, respectively (Fig. 5B).

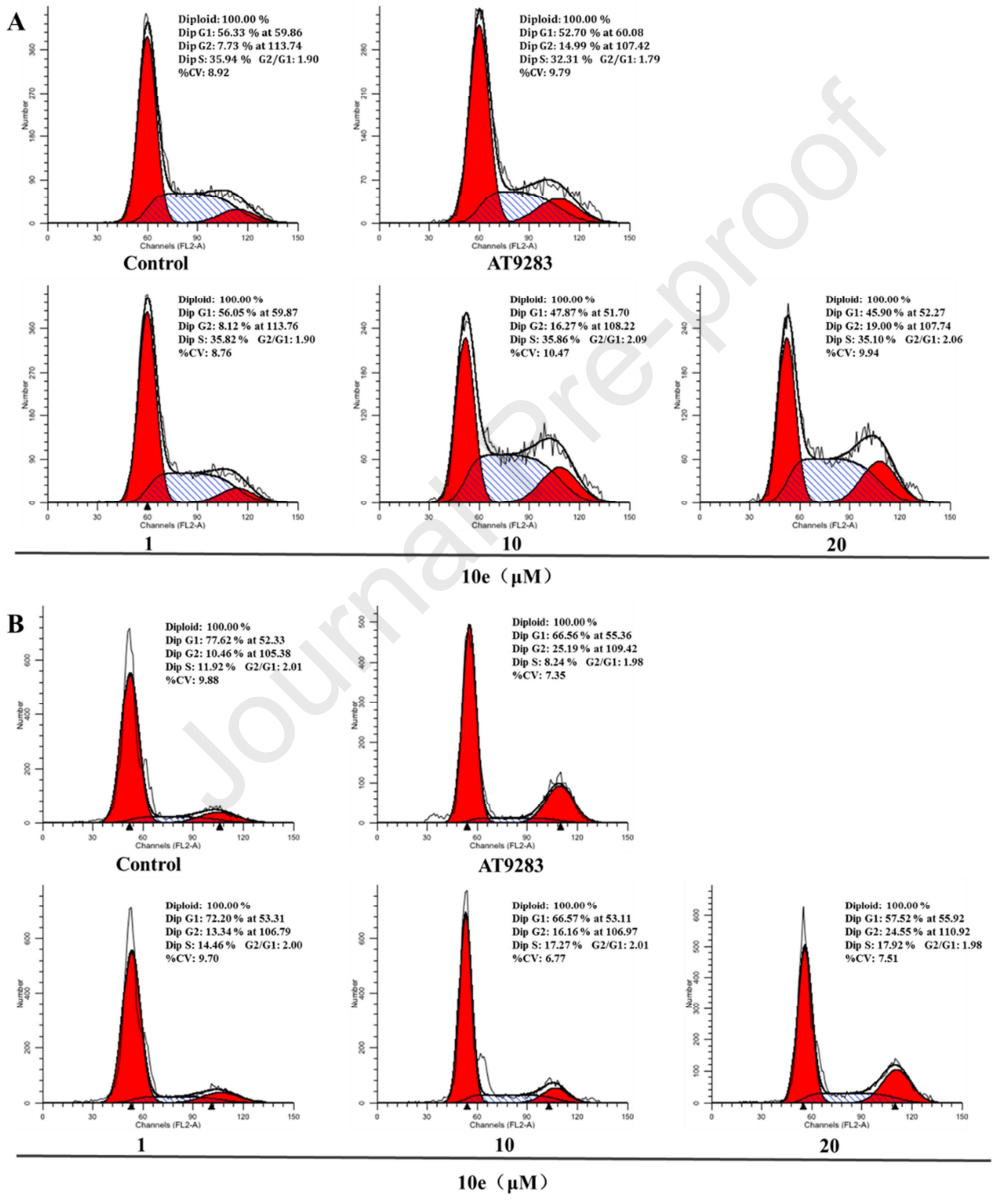

Fig. 5 compound **10e** induced cell cycle arrest at G2 phase in K562 and HCT116 cells.

2.3 Binding mechanism of **10e** to the JAK2, JAK3, Aurora A and Aurora B

Considering the above-mentioned integrated molecular modeling approach, RMSDs of kinase backbone atoms (Fig S3) and ligand heavy atoms (Fig S4) of the initial structures were calculated to assess the stability of the complex. In comparison to AT9832, the binding of **10e** induced large fluctuations of kinases (Fig S3), indicating that the binding of **10e** was less stable than AT9832, and also the stability of **10e** in these kinases was less than that of AT9832 (Fig S4). The above results were very consistent with our experimental data, which represented the lower binding affinities of **10e** (Table 4). These results encouraged us to explore the binding mechanism of **10e** further, by analyzing the MD trajectories.

To explore the binding mechanism of **10e** to kinases, MM-GBSA was employed to calculate the binding affinities of both **10e** and AT9832 with these kinases. The information on binding free energy obtained from MM-GBA calculations is given in Tables 4. The calculated differences of binding free energy between AT9832 and **10e** to JAK2, JAK3, Aurora A, and Aurora B were –2.85, –3.54, –1.71, and –1.61 kcal/mol, which were very consistent with the corresponding experimental data (-2.57, –2.30, –2.13 and –1.33 kcal/mol, respectively) (Table 4). The calculated difference of binding free energy between AT9832 and **10e** correlated properly to the experimental data ($R^2 = 0.48$, Fig S5). Thus, our current analysis of binding free energies could be considered as reliable.

As shown in Table 4, the van der Waals interactions (ΔEvdw), electrostatic interactions (ΔEele), and nonpolar solvation energies (ΔGsurf) were favorable for the binding of the ligands to kinases, while polar solvation energies (ΔGgb) heavily impaired the bindings. The van der Waals interaction was the main driving force for the binding of the inhibitors to kinases, which was consistent with the results of our previous simulations[52]. However, the electrostatic interactions (ΔEele+ΔGgb) between AT9832 and **10e** seemed to differ mostly. The differences of electrostatic interaction between AT9832 and **10e** to the JAK2, JAK3, Aurora A, and Aurora B were –11.48, –2.57, –1.62, and –0.61 kcal/mol. Thus, less electrostatic interactions of **10e** largely impaired the binding affinity of **10e**.

Table 4 Binding free energies of ligands (**10e** and AT9283) to JAK2, JAK3, Aurora A and Aurora B calculated using MM-GBSA method. The unit for binding free energy is kcal/mol.

		ΔGexp[a]	ΔGcal[b]	ΔEvdw	ΔEele	ΔEgb	ΔEsurf	ΔΔGcal[c]	ΔΔGexp[d]	ΔEele+ΔEgb
JAK2	**10e**	-9.30	-42.28	-52.70	-16.46	33.08	-6.20			
								-2.57	-2.85	-11.48
(2W1I)	AT9283	-11.87	-45.13	-44.92	-27.3	32.44	-5.34			
JAK3	**10e**	-9.94	-38.35	-42.65	-23.14	32.44	-4.99			
								-2.30	-3.54	-2.57
(3ZEP)	AT9283	-12.24	-41.88	-43.45	-27.47	34.20	-5.16			
Aurora A	**10e**	-8.27	-40.72	-43.40	-23.63	31.52	-5.19			
								-2.13	-1.71	-1.62
(2W1G)	AT9283	-10.40	-42.43	-43.48	-30.92	37.19	-5.2			
Aurora B	**10e**	-8.55	-41.31	-45.05	-26.13	36.89	-5.2			
								-1.33	-1.61	-0.61
(4AF3)	AT9283	-9.89	-42.92	-47.41	-23.19	33.35	-5.71			

[a] The experimental values were derived from the experimental *ki* values using the equation $\Delta G\text{exp} = -RT\ln IC_{50}$.

[b] $\Delta Gcal = \Delta E\text{ele} + \Delta E\text{vdw} + \Delta G\text{gb} + \Delta Gsurf$.

[c] $\Delta\Delta G_{cal}=\Delta G_{cal}$(AT9283)- ΔG_{cal}(**10e**).

[d] $\Delta\Delta G_{exp}=\Delta G_{exp}$(AT9283)- ΔG_{exp}(**10e**).

Next, snapshots from the last 150 ns trajectories were used for clustering to obtain a representative binding pose. As shown in Fig 6, the hydrogen bonds formed between the hinge region of the kinases and the compounds (AT9832 and **10e**) were the main interactions between ligands and kinases. For most of the kinases (JAK3, Aurora A, and Aurora B), the residues in the hinge could form three important hydrogen bonds between the ligands and the kinases. However, smaller distance and larger occupancy of these hydrogen bonds were identified in AT9832 than that of **10e** (Fig 6 and Table S1), suggesting that the interactions of AT9832 to the kinases were stronger than that of **10e** to the same kinases. In the case of JAK2, AT9832 formed three strong hydrogen bonds with the residues E930 and L932 in the hinge region with distances

of 2.8, 3.0, and 2.8 Å (Fig 6A), respectively. However, **10e** could form only one hydrogen bond between the residues E930 in the hinge region with a distance of 3.2 Å (Fig 6B). **10e** could form two other weaker hydrogen bonds to residues G993 and S936 of JAK2 (Fig 6B and Table S1). In summary, the current molecular modeling suggested that the **10e** could maintain a binding mode similar to AT9832, although it has a less binding affinity.

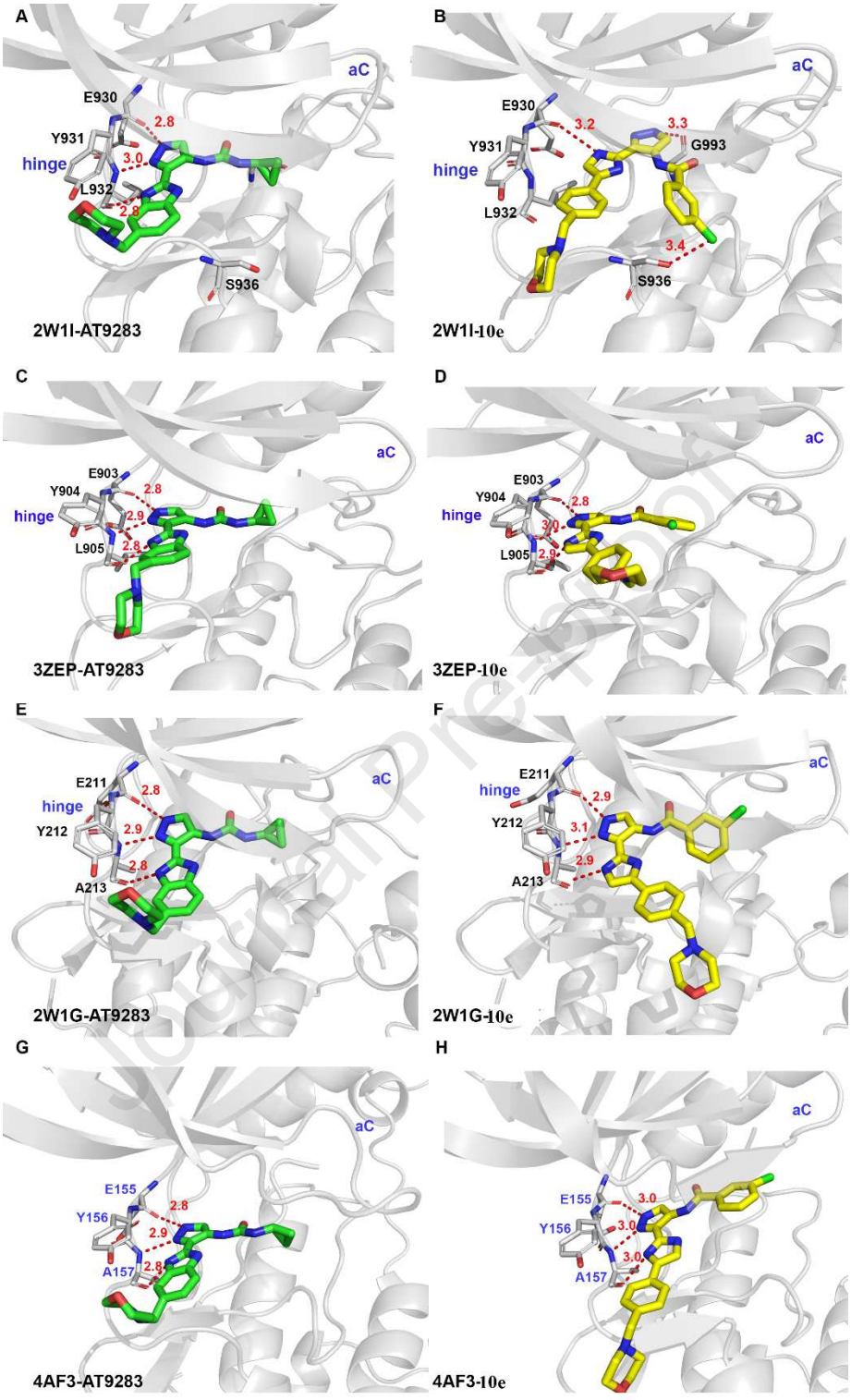

Fig 6 Binding pose of ligands (AT9283 and **10e**) to JAK2 (2W1I), JAK3 (3ZEP), Aurora A (2W1G) and Aurora B (4AF3), respectively. The important hydrogen bonds were plotted as red lines. The ligands and key residues were displayed in stick modes. The carbon atoms of AT9283 and **10e** were colored in green and yellow, respectively.

3. Conclusions

In summary, we designed and synthesized 3-(4-phenyl-1Himidazol-2-yl)-1H-pyrazole derivatives as potent JAK 2/3 and aurora A/B kinases multi-targeted inhibitors.

Most of the compounds exhibited potent inhibition against JAK2/3 and Aurora A/B with the IC_{50} values ranging from 0.008 to 2.52 μM. Among these derivatives, compound **10e** expressed the most moderate inhibiting activities against all the four kinases with the IC_{50} values, 0.166 μM (JAK2), 0.057 μM (JAK3), 0.939 μM(Aurora A), and 0.583 μM (Aurora B), respectively. Additionally, anti-proliferation assays shown that the compounds having a morpholine ring at the side chain (**10b-10e**) exhibited higher anti-proliferative activities against K562 and HTC116. In addition, **10e** has significantly lower toxic effect on human normal cells than JAK 2/3 and Aurora A/B kinases multi-target kinase inhibitor (AT9832). Furthermore, compound **10e** down-regulated the phosphorylation of STAT3, STAT5, Aurora A, and Aurora B in K562 and HCT116 cells. Cell cycle analysis revealed that compound **10e** inhibited the proliferation of cells by inducing cell cycle arrest in the G2 phase. The molecular modeling suggested that the **10e** could maintain a binding mode similar to AT9832, although it had a less binding affinity. Overall, compound **10e** is a potential anticancer agent that exhibits potent JAK 2/3 and aurora A/B kinases multi-targeted inhibitors.

4. Experimental

4.1. Chemistry

Unless otherwise noted, all reagents were purchased from commercial sources and used without further purification. All compounds were routinely monitored by thin-layer chromatography with silica gel GF-254 glass plates and viewed under UV light at 254 nm. The ^{1}H-NMR and ^{13}C-NMR spectra were determined in DMSO-d_6 on a JNM-ECZ400s/L spectrometer. Chemical shifts (δ) were reported in parts per million (ppm) relative to tetramethylsilane (TMS), which was used as an internal standard. The mass spectra (MS) were obtained from Agilent 1100LC/MS Spectrometry Services. HR-MS was obtained using a Q-tof high resolution mass spectrometer. The purity was obtained using Agilent 1260 HPLC instrument with ZORBAX SB-C18 chromatographic column. Melting point was obtained using X-4A

melting point analyzer.

*4.1.1 4-nitro-1-(tetrahydro-2H-pyran-2-yl)-1H-pyrazole-3-carboxylic acid (**2**)*

To a solution of 4-nitropyrazole-3-carboxylicacid (5.0 g，31.8 mmol) in THF (40 mL) was added 3,4-dihydro-2H-pyran (DHP, 8.04 g，95.5 mmol) and p-toluenesulfonic acid monohydrate (PTSA, 0.30 g，0.15 mmol). The reaction mixture was stirred at RT and monitored by thin layer chromatography. After completion of the reaction, the solvent was removed under vacuum and the product was dissolved in water (30 mL), and washed with acetic ether (3×20 mL). The organic layer was washed with saline (50 mL) and was dried (anhydrous sodium sulfate). The solvent was removed under vacuum and the crude product was purified by chromatographic column to afford 7.29 g compound **2**. Light yellow oil, yield: 95%.^{1}H NMR (400 MHz, $CDCl_3$-d_6) δ (ppm)：8.50 (s, 1H), 5.48 (d, J = 8.0 Hz, 1H), 4.11 (d, J = 12.0 Hz, 1H), 3.74 (t, J = 12.0 Hz, 1H), 2.29 (d, J = 11.8 Hz, 1H), 1.99 (s, 1H), 1.87 (d, J =8.0 Hz, 1H), 1.68 (s, 3H).

*4.1.2 1-(4-(bromomethyl)phenyl)ethan-1-one (**4**)*

The mixture of 4'-methylacetophenone (10 mL, 74.5 mmol), NBS(14.6 g, 82.0 mmol), AIBN(1.23 g, 7.49 mmol) and 80 mL acetonitrile was stirred at 90 ^{o}C under argon atmosphere for 4 h, then concentrated under vacuum to give a residue which was dissolved in water (30 mL) and washed with dichloromethane (3×50 mL). The dichloromethane solution was washed with 1 M hydrochloric acid solution (50 mL), saturated sodium bicarbonate solution and brine (3×50 mL), dried over anhydrous sodium sulfate and concentrated. The crude product was recrystallized from ethyl acetate (25.5 mL) and petroleum ether (255 mL) to afford 15.1g pure product. White solid, yield: 95%. ^{1}H NMR (400 MHz, $CDCl_3$-d_6) δ (ppm)： 7.92 (d, J = 8.1 Hz, 2H), 7.47 (d, J = 8.0 Hz, 2H), 4.49 (s, 2H), 2.60 (s, 3H).

*4.1.3 General procedure for the preparation of the compounds (**5**)*

To a solution of compound **4** (31.8 mmol) in acetonitrile (30 mL) was added potassium carbonate (23.5 mmol), catalytic amount of potassium iodide and different secondary amines (23.5 mmol). The reaction mixture was stirred at 90 ^{o}C for 4h, then concentrated under vacuum to give a residue which was purified by chromatographic column.

*4.1.3.1 1-(4-(morpholinomethyl)phenyl)ethan-1-one (**5a**)*

Yield: 90%. ^{1}H NMR (400 MHz, $CDCl_3$-d_6) δ (ppm)**:** 7.88 (d, *J* = 7.9 Hz, 2H), 7.41 (d, *J* = 7.8 Hz, 2H), 3.68 (s, 4H), 3.52 (s, 2H), 2.56 (s, 3H), 2.42 (s, 4H). HR-MS (calculated for $C_{13}H_{18}NO_2$ $(M+H)^+$ 220.1337; found 220.1334) (Figure 44).

*4.1.3.2 1-(4-(piperidin-1-ylmethyl)phenyl)ethan-1-one (**5b**)*

Yield: 90%. ^{1}H NMR (400 MHz, $CDCl_3$-d_6) δ (ppm)**:** 7.89 (d, *J* = 8.1 Hz, 2H), 7.41 (d, *J* = 8.0 Hz, 2H), 3.51 (s, 2H), 2.57 (s, 3H), 2.37 (s, 4H), 1.54 – 1.60 (m, 4H), 1.43 (d, *J* = 4.0 Hz, 2H). HR-MS (calculated for $C_{14}H_{20}NO$ $(M+H)^+$ 218.1545; found 218.1542)

*4.1.3.2 1-(4-(pyrrolidin-1-ylmethyl)phenyl)ethan-1-one (**5c**)*

Yield: 84%. ^{1}H NMR (400 MHz, $CDCl_3$-d_6) δ (ppm)**:** 7.88 (d, J = 7.9 Hz, 2H), 7.41 (d, J = 7.9 Hz, 2H), 3.65 (s, 2H), 2.57 (s, 3H), 2.50 (s, 4H), 1.77 (s, 4H). HR-MS (calculated for $C_{13}H_{18}NO$ $(M+H)^+$ 204.1388; found 204.1381).

*4.1.4 General procedure for the preparation of the compounds (**6**)*

To a solution of compound **5** (0.48mmol) in 48% HBr solution (2 mL) was added 0.96 mL bromine (0.5M in acetic acid) at 60 ^{o}C. After completion of the reaction, the solvent was removed under vacuum and the product was used for the next step without being purified.

*4.1.4 General procedure for the preparation of the compounds (**7**)*

To a solution of compound **2** (10 mmol), potassium carbonate (10 mmol) and catalytic amount of potassium in acetonitrile (10 mL) was added compound **6** (10 mmol) at RT. The mixture was stirred overnight, then filtered. The filtrate was removed under vacuum and the crude product was purified by chromatographic column to afford compound **7**.

*4.1.4.1 2-oxo-2-(4-(pyrrolidin-1-ylmethyl)phenyl)ethyl 4-nitro-1-(tetrahydro-2H-pyran-2-yl)-1H-pyrrole-3-carboxylate (**7c**)*

Yield: 63%. ^{1}H NMR (400 MHz, $CDCl_3$-d_6) δ (ppm)**:** 8.42 (s, 1H), 7.91 (d, *J* = 7.6 Hz, 2H), 7.53 (d, *J* = 7.6 Hz, 2H), 5.61 (s, 2H), 5.46 (d, *J* = 9.2 Hz, 1H), 4.09 (d, *J* = 11.6 Hz, 1H), 3.79 (s, 2H), 3.70 – 3.75 (m, 1H), 2.65 (s, 4H), 2.23-2.27 (m, 1H), 1.85 – 2.03 (m, 6H), 1.68 (s, 3H). HR-MS (calculated for $C_{22}H_{27}N_4O_6$ $(M+H)^+$ 443.1930;

found 443.1921).

*4.1.5 General procedure for the preparation of the compounds (**8**)*

To a solution of compound **7** (10 mmol) in acetic acid (30 mL) was added ammonium acetate (120 mmol). The mixture was stirred 130 ^{o}C for 4 h. Then the solvent was removed under vacuum and the residue was poured slowly into saturated sodium bicarbonate solution while stirring constantly. The solid formed was filtered off and purified by chromatographic column to afford compound **8**.

*4.1.5.1 4-(4-(2-(4-nitro-1H-pyrazol-3-yl)-1H-imidazol-4-yl)benzyl)morpholine (**8a**)*

Yellow solid, Yield: 46.2%. ^{1}H NMR (400 MHz, DMSO-*d*$_6$) δ (ppm)：8.59 (s, 1H), 7.78 (s, 3H), 7.29 (d, *J* = 4.0 Hz, 2H), 3.55 (s, 4H), 3.44 (s, 2H), 2.34 (s, 4H). HR-MS (calculated for $C_{17}H_{19}N_6O_3$ $(M+H)^+$ 355.1518; found 355.1512)

*4.1.6 General procedure for the preparation of the compounds (**9**)*

A solution of compound **8** (4 mmol) and 10% Pd/C (1.3mmol) in 40mL methanol under hydrogen was stirred at 40 ^{o}C for 12 h. Then the mixture was cool to RT, then filtered. The filtrate was removed under vacuum and the crude product was used for next step without being purified.

*4.1.7 General procedure for the preparation of the target compounds (**10a-10i**)*

To a solution of compound **9** (1.67 mmol) in dichloromethane (10 mL) was added triethylamine (2 mmol), then added the solution of acyl chloride (2 mmol) in dichloromethane (5 mL) drop by drop at 0 ^{o}C. The mixture was heated to RT and stirred for 4h. After completion of the reaction, the solvent was removed under vacuum and the residue was dissolved in water (10 mL) and extracted with acetic ether (3×20 mL). The acetic ether solution was washed with brine (50 mL), dried over anhydrous sodium sulfate and concentrated. The crude product was purified by chromatographic column to afford the target compounds.

4.1.7.1

*N-(3-(4-(4-(morpholinomethyl)phenyl)-1H-imidazol-2-yl)-1H-pyrazol-4-yl)benzamide (**10a**)*

While solid, yield 31.3%, Mp 220.7-221.3°C. ^{1}H NMR (400 MHz, DMSO-d_6) δ (ppm)： 11.55 (s, 1H), 8.29 (s, 1H), 8.04 (d, J = 7.6 Hz, 2H), 7.81 (d, J = 7.4 Hz, 2H), 7.59-7.67 (m, 4H), 7.33 (d, J = 7.4 Hz, 2H), 3.56 (s, 4H), 3.46 (s, 2H), 2.34 (s, 4H);^{13}C NMR (100 MHz, DMSO-d_6) δ (ppm)：163.23, 142.61, 140.34, 134.55, 134.42, 132.56, 131.95, 129.89, 129.51, 127.43, 127.30, 124.95, 124.72, 120.16, 120.03, 66.49, 62.62, 53.44; HR-MS (calculated for $C_{24}H_{25}N_6O_2$ $(M+H)^+$ 429.2039; found 429.2028); purity: 96.84%.

4.1.7.2

*4-methoxy-N-(3-(4-(4-(morpholinomethyl)phenyl)-1H-imidazol-2-yl)-1H-pyrazol-4-yl)benzamide (**10b**)*

While solid, yield 14.5 %, Mp 283.6-284.0°C. ^{1}H NMR (400 MHz, DMSO-d_6) δ (ppm)：12.98 (s, 1H), 12.97 (s, 1H), 11.42 (s, 1H), 8.26 (s, 1H), 7.99 (d, J = 8.8 Hz,2H), 7.81 (d, J = 8.4 Hz, 2H), 7.67 (s, 1H), 7.35 (d, J = 8.0 Hz, 2H), 7.12 (d, J = 8.8 Hz, 2H), 3.87 (s, 3H), 3.55 (t, J = 4.0 4H), 3.47 (s, 2H), 2.35 (s, 4H); ^{13}C NMR (100 MHz, DMSO-d_6) δ (ppm)：162.91, 162.67, 140.39, 136.61, 133.44, 129.86, 129.28, 129.12, 127.97, 126.70, 124.76, 120.41, 114.67, 113.64, 109.79, 66.77, 62.74, 56.05, 53.71; HR-MS (calculated for $C_{25}H_{27}N_6O_3$ $(M+H)^+$ 459.2144; found 459.2137); purity:97.83%.

4.1.7.3

*4-methoxy-N-(3-(4-(4-(morpholinomethyl)phenyl)-1H-imidazol-2-yl)-1H-pyrazol-4-yl)benzamide (**10c**)*

Yellow solid, yield 26.6 %, Mp 273.8-274.1°C. ^{1}H NMR (400 MHz, DMSO-d_6) δ (ppm)：13.09 (s, 1H), 12.96 (s, 1H), 11.71 (s, 1H), 8.39 (d, J = 8.4 Hz, 1H), 8.32 (s, 1H), 8.24 (d, J = 8.4 Hz, 1H), 7.78 (d, J = 7.6 Hz, 2H), 7.67 (s, 1H), 7.32 (d, J = 7.6 Hz, 2H), 3.56 (s, 4H), 3.46 (s, 2H), 2.35 (s, 4H); ^{13}C NMR (100 MHz, DMSO-d_6) δ (ppm)：161.63, 149.99, 142.41, 140.47, 140.09, 136.64, 133.32, 132.17, 129.77, 128.98, 124.86, 124.61, 120.47, 119.79, 113.71, 66.51, 62.90, 53.72; HR-MS (calculated for $C_{24}H_{24}N_7O_4$ $(M+H)^+$ 474.1890; found 474.1881); purity: 95.72%.

4.1.7.4

4-chloro-N-(3-(4-(4-(morpholinomethyl)phenyl)-1H-imidazol-2-yl)-1H-pyrazol-4-yl)b

*enzamide (**10d**)*

While solid, yield 23.6 %, Mp 296.7-297.1°C. ^{1}H NMR (400 MHz, DMSO-d_6) δ (ppm)：11.52 (s, 1H), 8.28 (s, 1H), 8.03 (d, J = 8.4 Hz, 2H), 7.78 (d, J = 8.0 Hz,2H), 7.66 (d, J = 8.0 Hz, 3H), 7.35 (d, J = 8.0 Hz, 2H), 3.56 (s, 4H), 3.47(s,2H), 2.35 (s, 4H); ^{13}C NMR (100 MHz, DMSO-d_6) δ (ppm)：162.28, 142.65, 140.45, 137.35, 133.44, 133.28, 131.98, 129.91, 129.55. 129.32, 129.21, 124.79, 120.24, 120.00, 113.62, 66.63, 62.80, 53.67; HR-MS (calculated for $C_{24}H_{24}ClN_6O_2$ $(M+H)^+$ 463.1649; found 463.1639) ; purity: 96.33%.

4.1.7.5

*3-chloro-N-(3-(4-(4-(morpholinomethyl)phenyl)-1H-imidazol-2-yl)-1H-pyrazol-4-yl)benzamide (**10e**)*

While solid, yield 27.3 %, Mp 266.4-266.8°C. ^{1}H NMR (400 MHz, DMSO-d_6) δ (ppm)：11.47 (s, 1H), 8.31 (s, 1H), 8.00 (s, 2H), 7.63-7.82 (m, 5H), 7.32 (d, J=4.8 Hz, 2H), 3.55 (s, 4H), 3.45 (s, 2H), 2.34 (s, 4H); ^{13}C NMR (100 MHz, DMSO-d_6) δ (ppm)：161.84, 142.63, 140.50, 136.44, 134.33, 133.40, 132.44, 132.04, 131.54, 129.89, 126.92, 126.46, 125.02, 124.71, 120.34, 119.86, 113.74, 66.49, 62.71, 53.65; HR-MS (calculated for $C_{24}H_{24}ClN_6O_2$ $(M+H)^+$ 463.1649; found 463.1630); purity: 95.26%.

4.1.7.6

*4-nitro-N-(3-(4-(4-(pyrrolidin-1-ylmethyl)phenyl)-1H-imidazol-2-yl)-1H-pyrazol-4-yl)benzamide (**10f**)*

Yellow solid, yield 23.6 %. ^{1}H NMR (400 MHz, DMSO-d_6) δ (ppm)：13.10 (s, 1H), 11.60 (s, 1H), 10.78 (s, 1H), 8.43 (d, J = 8.4 Hz, 2H), 8.37 (s, 1H), 8.29 (d, J = 8.0 Hz, 2H), 7.93 (d, J = 8.0 Hz, 2H), 7.84 (s, 1H), 7.64 (d, J = 8.0 Hz, 2H), 4.37(d, J = 4.4 Hz, 2H), 3.08 (s, 2H), 2.50 (s, 2H), 2.03 (s, 1H), 1.89 (s, 1H); ^{13}C NMR (100 MHz, DMSO-d_6) δ (ppm)：161.65, 149.98, 142.62, 140.14, 140.07, 134.53, 132.13, 130.73, 129.00, 125.00, 124.79, 124.42, 120.72, 119.89, 114.34, 58.36, 53.38, 23.30; HR-MS (calculated for $C_{24}H_{24}N_7O_3$ $(M+H)^+$ 458.1949; found 458.1937).

4.1.7.7

4-methoxy-N-(3-(4-(4-(piperidin-1-ylmethyl)phenyl)-1H-imidazol-2-yl)-1H-pyrazol-4-

*yl)benzamide (**10g**)*

While solid, yield 18.3 %, Mp 242.7-243.4°C. ^{1}H NMR (400 MHz, DMSO-d_6) δ (ppm)：11.42 (s, 1H), 8.26 (s, 1H), 8.00 (d, J = 8.4 Hz, 2H), 7.81 (d, J = 8.0 Hz, 2H), 7.66 (s, 1H), 7.34 (d, J = 7.6 Hz, 2H), 7.11 (d, J = 8.4 Hz, 2H), 3.86 (s, 3H), 3.46 (s, 2H), 2.34 (s, 4H), 1.48 (s, 4H), 1.36 (s, 2H); ^{13}C NMR (100 MHz, DMSO-d_6) δ (ppm)：162.90, 162.61, 142.75, 140.42, 133.38, 131.79, 129.81, 129.30, 129.18, 126.73, 124.70, 120.38, 119.82, 114.65, 113.58, 62.63, 56.04, 54.30, 25.99, 24.45; HR-MS (calculated for $C_{26}H_{29}N_6O_2$ $(M+H)^+$ 457.2352; found 457.2346); purity: 97.20%.

4.1.7.8

*4-chloro-N-(3-(4-(4-(piperidin-1-ylmethyl)phenyl)-1H-imidazol-2-yl)-1H-pyrazol-4-yl)benzamide (**10h**)*

While solid, yield 14.2 %, Mp 292.8-293.1°C. ^{1}H NMR (400 MHz, DMSO-d_6) δ (ppm)：11.43 (s, 1H), 10.66 (s, 1H), 8.34 (s, 1H), 8.01 – 8.05 (m, 2H), 7.96 (d, J = 8.0 Hz, 2H), 7.84 (s, 1H), 7.76 (d, J = 8.0 Hz, 1H), 7.71 (d, J = 8.0 Hz, 1H), 7.66 (d, J = 7.6 Hz, 2H), 4.25 (s, 2H), 3.33 (s, 3H), 2.83 (s, 2H), 1.67-1.78 (m, 5H), 1.36 (s, 1H); ^{13}C NMR (100 MHz, DMSO-d_6) δ (ppm)：161.15, 142.20, 139.22, 135.67, 134.79, 133.70, 131.67, 131.24, 130.86, 126.20, 125.76, 124.20, 119.69, 119.16, 114.04, 58.60, 51.35, 22.05, 21.35; HR-MS (calculated for $C_{25}H_{26}ClN_6O$ $(M+H)^+$ 461.1856; found 461.1850); purity: 99.50%.

4.1.7.9

*3-chloro-N-(3-(4-(4-(piperidin-1-ylmethyl)phenyl)-1H-imidazol-2-yl)-1H-pyrazol-4-yl)benzamide (**10i**)*

While solid, yield 19.4%, Mp 259.9-261.3°C. ^{1}H NMR (400 MHz, DMSO-d_6) δ (ppm)：11.43 (s, 1H), 10.68 (s, 1H), 8.34 (s, 1H), 8.01 – 8.05 (m, 2H), 7.96 (d, J = 8.0 Hz, 2H), 7.84 (s, 1H), 7.76 (d, J = 8.0 Hz, 1H), 7.71 (d, J = 8.0 Hz, 1H), 7.66 (d, J = 7.6 Hz, 2H), 4.25 (s, 2H), 3.29 (s, 2H), 2.84 (s, 2H), 1.78 (s, 4H), 1.67 (s, 1H), 1.36 (s, 1H); ^{13}C NMR (100 MHz, DMSO-d_6) δ (ppm)：161.15, 142.20, 139.22, 135.67, 134.79, 133.70, 131.67, 131.24, 130.86, 126.20, 125.76, 124.41, 124.20, 119.69, 119.48, 119.26, 114.04, 58.60, 51.35, 22.05, 21.35; HR-MS (calculated for

$C_{25}H_{26}ClN_6O$ $(M+H)^+$ 461.1856; found 461.1836); purity: 97.01%.

4.1.8

*6-chloro-2-methyl-N-(3-(4-(4-(morpholinomethyl)phenyl)-1H-imidazol-2-yl)-1H-pyrazol-4-yl)pyrimidin-4-amine (**10j**)*

The mixture of compound 9 (0.32 g, 1.0 mmol), 4,6-dichloro-2-methylpyrimidine (0.13 g, 0.83 mmol), sodium iodide (0.15g, 1.0 mmol), N,N-diisopropylethylamine (0.13 g, 1.0 mmol) and 3 mL DMF was stirred at 90 ^oC under argon atmosphere for 4 h. Then the mixture was cool to RT, poured in ice water (30 mL) and stirred for 30 min. The solid formed was filtered off and purified by chromatographic column to afford 0.131g compound **10j**.

While solid, yield 29.5%, Mp 287.2-287.7^oC.^1H NMR (400 MHz, DMSO-d_6) δ (ppm)：10.02 (s, 1H), 8.37 (s, 1H), 7.84 (d, *J* = 7.2 Hz, 1H), 7.78 (d, *J* = 8.0 Hz, 1H), 7.63 (s, 1H), 7.30 (d, *J* = 7.6 Hz, 2H), 6.90 (s, 1H), 3.55 (s, 4H), 3.44 (s, 2H), 2.46 – 2.47(m, 3H), 2.34 (s, 4H); ^{13}C NMR (100 MHz, DMSO-d_6) δ (ppm)：168.46, 168.37, 164.49, 160.37, 142.33, 140.52, 136.27, 133.40, 129.88, 129.77, 124.90, 120.98, 120.11, 113.48, 66.51, 62.93, 53.71, 25.87; HR-MS (calculated for $C_{22}H_{24}ClN_8O$ $(M+H)^+$ 451.1761; found 451.1753); purity: 99.64%.

*4.1.9 1-(4-(3-chloropropoxy)phenyl)ethan-1-one (**12**)*

To the solution of 4'-hydroxyacetophenone (1.36 g, 10 mmol) and 1-bromo-3-chloropropane (1.56 g, 10 mmol) in 10mL acetonitrile was added potassium carbonate (1.38g, 10 mmol) and catalytic amount of potassium. The mixture as stirred at 85 ^oC for 4 h, then was cool to RT and filtered. The filtrate was removed under vacuum and the crude product was purified by chromatographic column to afford 2.02 g compound **12** (yield 95.2%).^1H NMR (400 MHz, $CDCl_3$-d_6) δ (ppm)：δ 7.91 (d, *J* = 7.8 Hz, 2H), 6.91 (d, *J* = 7.9 Hz, 2H), 4.16 (t, *J* = 6.0 Hz, 2H), 3.73 (t, *J* = 5.6 Hz, 2H), 2.53 (s, 3H), 2.21 – 2.27 (m, 2H); HR-MS (calculated for $C_{11}H_{14}O_2Cl$ $(M+H)^+$ 213.0682; found 213.0677).

*4.1.10 1-(4-(3-morpholinopropoxy)phenyl)ethan-1-one (**13**)*

To a solution of compound **12** (2.12 g, 10 mmol) and morpholine (0.87 g, 10 mmol) in acetonitrile (10 mL) was added potassium carbonate (1.38g, 10 mmol), catalytic

amount of potassium iodide. The reaction mixture was stirred at 85 ^{o}C for 4h, then concentrated under vacuum and the residue was purified by chromatographic column to give 2.2g compound **13** (yield 83.6 %).^{1}H NMR (400 MHz, $CDCl_3$-*d6*) δ (ppm)：7.89 (d, *J* = 8.1 Hz, 2H), 6.90 (d, *J* =12 Hz, 2H), 3.99 - 4.08 (m, 1H), 3.63 - 3.70 (m, 3H), 2.48 – 2.52 (m, 3H), 2.39-2.45 (m, 4H), 1.91 - 2.00 (m, 2H); HR-MS (calculated for $C_{15}H_{22}NO_3$ $(M+H)^+$ 264.1599; found 264.1596) (Figure 56).

*4.1.11 2-bromo-1-(4-(3-morpholinopropoxy)phenyl)ethan-1-one (**14**)*

To a solution of compound **13** (2.63 g, 10 mmol) in 48% HBr solution (20 mL) was added 20 mL solution of bromine in acetic acid(0.5M) at 60 ^{o}C. After completion of the reaction, the solvent was removed under vacuum and the product was used for the next step without being purified.

*4.1.12 2-(4-(3-morpholinopropoxy)phenyl)-2-oxoethyl 4-nitro-1H-pyrazole-3-carboxylate (**15**)*

To a solution of compound **2** (2.41g, 10 mmol), potassium carbonate (1.38g, 10 mmol) and catalytic amount of potassium in acetonitrile (10 mL) was added compound **14** (4.21g, 10 mmol) at RT. The mixture was stirred overnight, then filtered. The filtrate was removed under vacuum and the crude product was purified by chromatographic column to afford 3.26g compound **15** (yield 65.0%).^{1}H NMR (400 MHz, $CDCl_3$-*d6*) δ (ppm)：8.40 (s, 1H), 7.90 (d, *J* = 8.0 Hz, 2H), 6.94 (d, *J* = 8.0 Hz, 2H), 5.57 (s, 2H), 5.45 (d, *J* = 8.0 Hz, 1H), 4.09 (t, *J* = 8.0 Hz, 3H), 3.71 (s, 5H), 2.53 (t, *J* = 8.0 Hz, 3H), 2.48 (s, 3H), 2.20 – 2.25 (m, 1H), 1.87 – 2.01 (m, 4H), 1.66 (s, 3H); HR-MS (calculated for $C_{24}H_{31}N_4O_8$ $(M+H)^+$ 503.2142; found 503.2130).

*4.1.13 2-(4-(3-morpholinopropoxy)phenyl)-2-oxoethyl 4-nitro-1H-pyrazole-3-carboxylate (**16**)*

To a solution of compound **15** (5.02g, 10 mmol) in acetic acid (25 mL) was added ammonium acetate (9.24g, 120 mmol). The mixture was stirred 125 ^{o}C for 4 h. Then the solvent was removed under vacuum and the residue was poured slowly into saturated sodium bicarbonate solution while stirring constantly. The solid formed was filtered off and used for next step without being purified.

4.1.14 2-(4-(3-morpholinopropoxy)phenyl)-2-oxoethyl

*4-nitro-1H-pyrazole-3-carboxylate (**17**)*

A solution of compound **16** (1.59g, 4 mmol) and 10% Pd/C (0.14g, 1.3mmol) in 40mL methanol under hydrogen was stirred at 40 ^{o}C for 12 h. Then the mixture was cool to RT, then filtered. The filtrate was removed under vacuum and the crude product was used for next step without being purified.

*4.1.15 General procedure for the preparation of the target compounds (**18a**)*

The mixture of compound **17** (1.0 mmol), chlor pyrimidine derivative (0.83 mmol), sodium iodide (0.15g, 1.0 mmol), N,N-diisopropylethylamine (0.13 g, 1.0 mmol) and 5 mL DMF was stirred at 90 ^{o}C under argon atmosphere for 4 h. Then the mixture was cool to RT, poured in ice water (50 mL) and stirred for 30 min, and extracted with ethyl acetate (3×40 mL). The combined organic layer was washed with brine (2×100 mL) and dried (Na_2SO_4). The solvent was removed under vacuum and the product was purified by chromatographic column.

*4.1.15.1 6-chloro-5-methyl-2-(methylthio)-N-(3-(5-(4-(3-morpholinopropoxy) phenyl)-1H-imidazol-2-yl)-1H-pyrazol-4-yl) pyrimidin-4-amine (**18a**)*

While solid, yield 24.0%, Mp 245.3-245.9^{o}C. ^{1}H NMR (400 MHz, DMSO-d_6) δ (ppm)：δ 10.38 (s, 1H), 8.30 (s, 1H), 7.74 (d, *J* = 8.0 Hz, 2H), 7.55 (s, 1H), 6.94 (d, *J* = 8.0 Hz, 2H), 4.01 (t, *J* = 4.0 Hz, 2H), 3.56 (s, 4H), 2.53 (s, 5H), 2.28 – 2.40(m, 7H), 1.87 (s, 2H); ^{13}C NMR (100 MHz, DMSO-d_6) δ (ppm)：168.76, 158.08, 156.58, 143.25, 142.40, 140.58, 127.31, 126.61, 126.21, 120.54, 119.88, 115.10, 112.58, 107.52, 66.58, 66.28, 55.36, 53.82, 26.32, 14.34, 13.04; HR-MS (calculated for $C_{25}H_{30}N_8O_2SCl$ $(M+H)^+$ 541.1901; found 541.1897); purity: 99.72%.

4.2. Biological evaluation

4.2.1 *In vitro* kinases assays

Theses assays were carried out as described previously[53]. All of the enzymatic reactions were conducted at 30℃ for 40 minutes. The 50μl reaction mixture contains 40 mM Tris, pH 7.4, 10 mM $MgCl_2$, 0.1 mg/ml BSA, 1 mM DTT, 10 μM ATP, Kinase and the enzyme substrate. The compounds were diluted in 10% DMSO and 5μl of the dilution was added to a 50μl reaction so that the final concentration of DMSO is 1% in all of reactions. The assay was performed using Kinase-Glo Plus luminescence

kinase assay kit. It measures kinase activity by quantitating the amount of ATP remaining in solution following a kinase reaction. The luminescent signal from the assay is correlated with the amount of ATP present and is inversely correlated with the amount of kinase activity. The IC_{50} values were calculated using nonlinear regression with normalized dose-response fit using Prism GraphPad sofeware.

4.2.2 *In vitro* anti-proliferative assays

The cytotoxicity of each compound was determined using CCK-8 assay. Cells were seeded in 96-well plates and then treated with different concentrations of drugs. After 72 h of incubation, CCK-8 staining was performed to determine the OD value and calculate the inhibition rate. The IC_{50} values were calculated by using LOGIT method.

4.2.3 Western blot

Western blot analysis was performed according to previously published researches [44-47]. Cells were treated with compounds at different concentrations for 48h, then harvested and washed in ice-cold PBS, added cold RIPA buffer. The cells were centrifuged and the supernatant was collected as whole cell lysate. Protein concentration was determined by BCA method. Western blot analyses were conducted after separation by SDS/PAGE electrophoresis and transfer to nitrocellulose filter membrane. After blocking the membranes with 5% fat-free milk, primary antibody was added, shocked at 4 ^{o}C for overnight and washed with TBST. Then second antibody was added, shocked for 1h, washed with TBST. GAPDH was used as a loading control. The protein bands were visualized using the G: BOX chemiXR5.

4.2.4 Cell cycle assays

Cells were treated with compounds at different concentrations for 48h and washed with PBS twice. 5×10^5 cells were collected, added 100 μL RNase A at 37 ^{o}C for 30 min, stained with propidium iodide (400μL) at 4 ^{o}C for 30 min and then analyzed using flow cytometry.

4.3 Binding mechanism explored by molecular modeling

In order to explore the binding mechanism of our active compound **10e**, an integrated molecular modeling approach, which combines the docking calculation and molecular dynamics (MD) simulations, was performed (Fig S1). Initial ligand-protein complex

structures were obtained using the Autodock Vina. The best binding pose obtained from AutoDock Vina was selected for further refinement using MD simulations. The final binding pose was identified by clustering the trajectories from MD simulations.

AutoDock Vina (version 1.1.2) [54], which is a widely used molecular docking and virtual screening application , was selected to predict the binding pose of our active compound MZ-1E to the JAK2, JAK3, Aurora A and Aurora B, respectively. The compound AT9832 was chosen as reference. Corresponding X-ray structures of JAK2, JAK3, Aurora A and Aurora B were download from PDB with ID of 2W1I[55], 3ZEP[56], 2W1G[55] and 4AF3[57], respectively. All non-protein atoms including water and ligand in the X-ray structures were deleted and polar hydrogen atoms were added using MGLTools (version 1.5.6) [58]. The center of the ligand in the X-ray structures was used as target binding site grid center for docking. SMILES of **10e** and AT9832 were converted to the PDBQT format using Open Babel (version 2.3.2) [59] with the following options: --gen3d and -p 7.0. Then, docking calculations were performed with AutoDock Vina to obtain the initial binding pose. The exhaustiveness parameter was set to 30. In order to validate the parameters and software, the compound AT9832 with experimental structures was docked into JAK2 and AURKA, respectively. The root mean square deviations (RMSDs) of the AT9832 between the calculated and crystal determined one are very small (below 1.0 Å) (Fig S2), suggesting our docking protocol is reliable.

Then, the best docking models of each system were used as initial structure for MD simulations. The missing hydrogen atoms were added using *tleap* in AMBER18 [60]. The ff14SB force field [61] and GAFF[62] were employed to model the protein and ligand, respectively. The kinase-ligand complex was solvated in a cubic box of TIP3P water molecules [63] with a minimum distance of 10 Å between the protein surface and box edge. The system was first energy minimized with 2 kcal/(mol $Å^2$) harmonic position restraints applied on the heavy atoms of protein and ligand. Then, the system was heated from 0 to 300 K in the constant volume and temperature (NVT) canonical ensemble for 1 ns, imposing position restraints of 2.0 kcal/(mol $Å^2$) on the

heavy atoms of protein and ligand. The system was further equilibrated in the isothermal−isobaric (NPT) ensemble for 1 ns, reducing the position restraints to 1.0 kcal/(mol Å^2). Finally, 300 ns production MD simulations were carried out in the NPT ensemble without any constraints. All the simulations were performed using the GPU version of AMBER18 [60]. The bond lengths of hydrogen–heavy atoms were constrained using the SHAKE algorithm [64]. A distance cutoff of 9.0 Å was used for the van der Waals and short-range electrostatic interactions. Long-range electrostatic interactions were computed with the particle-mesh Ewald summation method [65]. A 2-fs integration time step was used in all MD simulations.

The MD simulations became stable after 150 ns as there were small fluctuations in the protein backbone RMSDs from 150 ns to 300 ns (Fig S3). Thus, snapshots were extracted from the last 150ns MD trajectories to obtain refined binding pose and binding free energy (ΔG) calculation with MM/GBSA approach. The ΔG in the MM/GBSA approach was calculated according to equation (1),

$$\Delta \mathrm{G}_{binding} = \Delta \mathrm{H} - \mathrm{T}\Delta \mathrm{S} = \Delta E_{ele} + \Delta E_{vdw} + \Delta G_{gb} + \Delta G_{surf} - T\Delta S \quad (1)$$

where ΔE_{vdw} and ΔE_{ele} were the non-bonded van der Waals and electrostatic interaction energies between the ligands and kinases in the gas phase, respectively. The ΔG_{gb} and ΔG_{surf} were the polar and non-polar interaction energies between the ligand and protein, respectively. The ΔG_{gb} was computed using the *pbsa* program in Amber 18[60]. The dielectric constants of solvent and solute were set to 80.0 and 1.0, respectively. The OBC solvation model[66] was used in this study. The ΔG_{surf} term was calculated as:

$$\Delta G_{surf} = \gamma * SASA + \beta \quad (2)$$

where SASA was the solvent accessible surface area as computed using the MSMS program [67]. The γ and β coefficients were set to 0.0072 kcal/(mol Å^2) and 0 kcal/mol, respectively. The fluctuation of entropy is quite large, thus we do not include this energy term in the current study.

Acknowledgment

The authors are grateful for the financial support by National Natural Science Foundation of China (81602951); Natural Science Foundation of Jiangsu Province

(BK20130216); Six talent peaks project in Jiangsu Province(2016-SWYY-062); Science and technology project of Xuzhou City (KC16SG255).

References

[1] L.Y. Shi, Z.P. Zhong, X.T. Li, Y.Q. Zhou, Z.Y. Pan, Discovery of an Orally Available Janus Kinase 3 Selective Covalent Inhibitor, Journal of Medicinal Chemistry, 62 (2019) 1054-1066.

[2] W.Q. Wang, Y.Y. Diao, W.J. Li, Y.T. Luo, T.Y. Yang, Y.Y. Zhao, T.T. Qi, F.L. Xu, X.Y. Ma, H. Ge, Y.F. Liang, Z.J. Zhao, X. Liang, R. Wang, L.L. Zhu, H.L. Li, Y.F. Xu, Design, synthesis and structure-activity relationship study of aminopyridine derivatives as novel inhibitors of Janus kinase 2, Bioorganic & Medicinal Chemistry Letters, 29 (2019) 1507-1513.

[3] M.S.A. Elsayed, J.J. Nielsen, S. Park, J. Park, Q.Y. Liu, C.H. Kim, Y. Pommier, K. Agama, P.S. Low, M. Cushman, Application of Sequential Palladium Catalysis for the Discovery of Janus Kinase Inhibitors in the Benzo c pyrrolo 2,3-h 1,6 naphthyridin-5-one (BPN) Series, Journal of Medicinal Chemistry, 61 (2018) 10440-10462.

[4] P. Coppo, S. Flamant, V. De Mas, P. Jarrier, M. Guillier, M.-L. Bonnet, C. Lacout, F. Guilhot, W. Vainchenker, A.G. Turhan, BCR-ABL activates STAT3 via JAK and MEK pathways in human cells, British Journal of Haematology, 134 (2006) 171-179.

[5] J.H. Jung, T.-R. Kwon, S.-J. Jeong, E.-O. Kim, E.J. Sohn, M. Yun, S.-H. Kim, Apoptosis Induced by Tanshinone IIA and Cryptotanshinone Is Mediated by Distinct JAK/STAT3/5 and SHP1/2 Signaling in Chronic Myeloid Leukemia K562 Cells, Evidence-Based Complementary and Alternative Medicine, (2013).

[6] R.R. Nair, J.H. Tolentino, R.F. Argilagos, L. Zhang, J. Pinilla-Ibarz, L.A. Hazlehurst, Potentiation of Nilotinib-mediated cell death in the context of the bone marrow microenvironment requires a promiscuous JAK inhibitor in CML, Leukemia Research, 36 (2012) 756-763.

[7] A.S.Y. Saglam, E. Alp, Z. Elmazoglu, S. Menevse, Treatment with cucurbitacin B alone and in combination with gefitinib induces cell cycle inhibition and apoptosis via EGFR and JAK/STAT pathway in human colorectal cancer cell lines, Human & Experimental Toxicology, 35 (2016) 526-543.

[8] H.-X. Tan, Z.-B. Cao, T.-T. He, T. Huang, C.-L. Xiang, Y. Liu, TGF beta 1 is essential for MSCs-CAFs differentiation and promotes HCT116 cells migration and invasion via JAK/STAT3 signaling, Oncotargets and Therapy, 12 (2019) 5323-5334.

[9] S.-W. Wang, J. Hu, Q.-H. Guo, Y. Zhao, J.-J. Cheng, D.-S. Zhang, Q. Fei, J. Li, Y.-M. Sun, AZD1480, a JAK inhibitor, inhibits cell growth and survival of colorectal cancer via modulating the JAK2/STAT3 signaling pathway, Oncology Reports, 32 (2014) 1991-1998.

[10] X.M. Lin, H. Chen, X.L. Zhan, MiR-203 regulates JAK-STAT pathway in affecting pancreatic cancer cells proliferation and apoptosis by targeting SOCS3, European Review for Medical and Pharmacological Sciences, 23 (2019) 6906-6913.

[11] T.B. Toh, J.J. Lim, L. Hooi, M.B.M.A. Rashid, E.K.-H. Chow, Targeting Jak/Stat pathway as a therapeutic strategy against SP/CD44+ tumorigenic cells in Akt/beta-catenin-driven hepatocellular carcinoma, Journal of hepatology, (2019).

[12] S. Wang, S. Zhang, Y. He, X. Huang, Y. Hui, Y. Tang, HOXA11-AS regulates JAK-STAT pathway by miR-15a-3p/STAT3 axis to promote the growth and metastasis in liver cancer, Journal of Cellular Biochemistry, 120 (2019) 15941-15951.

[13] W. Wen, E.S. Han, T.H. Dellinger, J. Wu, Y. Guo, R. Buettner, D.A. Horne, R. Jove, J.H. Yim, Increasing Antitumor Activity of JAK Inhibitor by Simultaneous Blocking Multiple Survival Signaling Pathways in Human Ovarian Cancer, Translational Oncology, 12 (2019) 1015-1025.

[14] D. Zhu, Y. Yu, W. Wang, K. Wu, D. Liu, Y. Yang, C. Zhang, Y. Qi, S. Zhao, Long noncoding RNA PART1 promotes progression of non-small cell lung cancer cells via JAK-STAT signaling pathway, Cancer Medicine, (2019).

[15] C. Harrison, J.-J. Kiladjian, H.K. Al-Ali, H. Gisslinger, R. Waltzman, V. Stalbovskaya, M. McQuitty, D.S. Hunter, R. Levy, L. Knoops, F. Cervantes, A.M. Vannucchi, T. Barbui, G. Barosi, JAK Inhibition with Ruxolitinib versus Best Available Therapy for Myelofibrosis, New England Journal of Medicine, 366 (2012) 787-798.

[16] A.M. Vannucchi, J.J. Kiladjian, M. Griesshammer, T. Masszi, S. Durrant, F. Passamonti, C.N. Harrison, F. Pane, P. Zachee, R. Mesa, S. He, M.M. Jones, W. Garrett, J. Li, U. Pirron, D. Habr, S. Verstovsek, Ruxolitinib versus Standard Therapy for the Treatment of Polycythemia Vera, New England Journal of Medicine, 372 (2015) 426-435.

[17] S. Verstovsek, R.A. Mesa, J. Gotlib, R.S. Levy, V. Gupta, J.F. DiPersio, J.V. Catalano, M. Deininger, C. Miller, R.T. Silver, M. Talpaz, E.F. Winton, J.H. Harvey, Jr., M.O. Arcasoy, E. Hexner, R.M. Lyons, R. Paquette, A. Raza, K. Vaddi, S. Erickson-Viitanen, I.L. Koumenis, W. Sun, V. Sandor, H.M. Kantarjian, A Double-Blind, Placebo-Controlled Trial of Ruxolitinib for Myelofibrosis, New

England Journal of Medicine, 366 (2012) 799-807.

[18] L. Xing, Z. Dai, A. Jabbari, J.E. Cerise, C.A. Higgins, W. Gong, A. de Jong, S. Harel, G.M. DeStefano, L. Rothman, P. Singh, L. Petukhova, J. Mackay-Wiggan, A.M. Christiano, R. Clynes, Alopecia areata is driven by cytotoxic T lymphocytes and is reversed by JAK inhibition, Nature Medicine, 20 (2014) 1043-1049.

[19] A. Quintas-Cardama, H. Kantarjian, J. Cortes, S. Verstovsek, Janus kinase inhibitors for the treatment of myeloproliferative neoplasias and beyond, Nature Reviews Drug Discovery, 10 (2011) 127-140.

[20] S. Ioannidis, M.L. Lamb, T. Wang, L. Almeida, M.H. Block, A.M. Davies, B. Peng, M. Su, H.-J. Zhang, E. Hoffmann, C. Rivard, I. Green, T. Howard, H. Pollard, J. Read, M. Alimzhanov, G. Bebernitz, K. Bell, M. Ye, D. Huszar, M. Zinda, Discovery of 5 Chloro-N-2-(1S)-1-(5-fluoropyrimidin-2-yl)ethyl -N-4-(5-methyl-1H-pyraz ol-3-yl)pyrimidine-2,4-diamine (AZD1480) as a Novel Inhibitor of the Jak/Stat Pathway, Journal of Medicinal Chemistry, 54 (2011) 262-276.

[21] A. Pardanani, C. Harrison, J.E. Cortes, F. Cervantes, R.A. Mesa, D. Milligan, T. Masszi, E. Mishchenko, E. Jourdan, A.M. Vannucchi, M.W. Drummond, M. Jurgutis, K. Kuliczkowski, E. Gheorghita, F. Passamonti, F. Neumann, A. Patki, G. Gao, A. Tefferi, Safety and Efficacy of Fedratinib in Patients With Primary or Secondary Myelofibrosis A Randomized Clinical Trial, Jama Oncology, 1 (2015) 643-651.

[22] H.T. Arkenau, R. Plummer, L.R. Molife, D. Olmos, T.A. Yap, M. Squires, S. Lewis, V. Lock, M. Yule, J. Lyons, H. Calvert, I. Judson, A phase I dose escalation study of AT9283, a small molecule inhibitor of aurora kinases, in patients with advanced solid malignancies, Annals of Oncology, 23 (2012) 1307-1313.

[23] M. Carmena, W.C. Earnshaw, The cellular geography of aurora kinases, Nature Reviews Molecular Cell Biology, 4 (2003) 842-854.

[24] N. Keen, S. Taylor, Aurora-kinase inhibitors as anticancer agents, Nat. Rev. Cancer, 4 (2004) 927-936.

[25] J.R. Bischoff, L. Anderson, Y.F. Zhu, K. Mossie, L. Ng, B. Souza, B. Schryver, P. Flanagan, F. Clairvoyant, C. Ginther, C.S.M. Chan, M. Novotny, D.J. Slamon, G.D. Plowman, A homologue of Drosophila aurora kinase is oncogenic and amplified in human colorectal cancers, Embo Journal, 17

(1998) 3052-3065.

[26] J. Fu, M. Bian, Q. Jiang, C. Zhang, Roles of aurora kinases in mitosis and tumorigenesis, Molecular Cancer Research, 5 (2007) 1-10.

[27] X.-F. Huang, S.-K. Luo, J. Xu, J. Li, D.-R. Xu, L.-H. Wang, M. Yan, X.-R. Wang, X.-B. Wan, F.-M. Zheng, Y.-X. Zeng, Q. Liu, Aurora kinase inhibitory VX-680 increases Bax/Bcl-2 ratio and induces apoptosis in Aurora-A-high acute myeloid leukemia, Blood, 111 (2008) 2854-2865.

[28] S. Wang, C.A. Midgley, F. Scaerou, J.B. Grabarek, G. Griffiths, W. Jackson, G. Kontopidis, S.J. McClue, C. McInnes, C. Meades, M. Mezna, A. Plater, I. Stuart, M.P. Thomas, G. Wood, R.G. Clarke, D.G. Blake, D.I. Zheleva, D.P. Lane, R.C. Jackson, D.M. Glover, P.M. Fischer, Discovery of N-Phenyl-4-(thiazol-5-yl)pyrimidin-2-amine Aurora Kinase Inhibitors, Journal of Medicinal Chemistry, 53 (2010) 4367-4378.

[29] M. Dennis, M. Davies, S. Oliver, R. D'Souza, L. Pike, P. Stockman, Phase I study of the Aurora B kinase inhibitor barasertib (AZD1152) to assess the pharmacokinetics, metabolism and excretion in patients with acute myeloid leukemia, Cancer Chemotherapy and Pharmacology, 70 (2012) 461-469.

[30] S. Geuns-Meyer, V.J. Cee, H.L. Deak, B. Du, B.L. Hodous, N. Hanh Nho, P.R. Olivieri, L.B. Schenkel, K.R. Vaida, P. Andrews, A. Bak, X. Be, P.J. Beltran, T.L. Bush, M.K. Chaves, G. Chung, Y. Dai, P. Eden, K. Hanested, L. Huang, M.-H.J. Lin, J. Tang, B. Ziegler, R. Radinsky, R. Kendall, V.F. Patel, M. Payton, Discovery of N-(4-(3-(2-Aminopyrimidin-4-yl)pyridin-2-yloxy)phenyl)-4-(4-methylthioph en-2-yl)phthalazin-1-amine (AMG 900), A Highly Selective, Orally Bioavailable Inhibitor of Aurora Kinases with Activity against Multidrug-Resistant Cancer Cell Lines, Journal of Medicinal Chemistry, 58 (2015) 5189-5207.

[31] P. Carpinelli, R. Ceruti, M.L. Giorgini, P. Cappella, L. Gianellini, V. Croci, A. Degrassi, G. Texido, M. Rocchetti, P. Vianello, L. Rusconi, P. Storici, P. Zugnoni, C. Arrigoni, C. Soncini, C. Alli, V. Patton, A. Marsiglio, D. Ballinari, E. Pesenti, D. Fancelli, J. Moll, PHA-739358, a potent inhibitor of Aurora kinases with a selective target inhibition profile relevant to cancer, Molecular Cancer Therapeutics, 6 (2007) 3158-3168.

[32] M.G. Manfredi, J.A. Ecsedy, K.A. Meetze, S.K. Balani, O. Burenkova, W. Chen, K.M. Galvin, K.M. Hoar, J.J. Huck, P.J. LeRoy, E.T. Ray, T.B. Sells, B. Stringer, S.G. Stroud, T.J. Vos, G.S. Weatherhead, D.R. Wysong, M. Zhang, J.B. Bolen, C.F. Claiborne, Antitumor activity of MLN8054, an

orally active small-molecule inhibitor of Aurora A kinase, Proceedings of the National Academy of Sciences of the United States of America, 104 (2007) 4106-4111.

[33] E.C. Dees, R.B. Cohen, M. von Mehren, T.E. Stinchcombe, H. Liu, K. Venkatakrishnan, M. Manfredi, H. Fingert, H.A. Burris, III, J.R. Infante, Phase I Study of Aurora A Kinase Inhibitor MLN8237 in Advanced Solid Tumors: Safety, Pharmacokinetics, Pharmacodynamics, and Bioavailability of Two Oral Formulations, Clinical Cancer Research, 18 (2012) 4775-4784.

[34] A.A. Dar, L.W. Goff, S. Majid, J. Berlin, W. El-Rifai, Aurora Kinase Inhibitors - Rising Stars in Cancer Therapeutics?, Molecular Cancer Therapeutics, 9 (2010) 268-278.

[35] J.Y. Zhu, T.J. Hou, X.L. Mao, Discovery of selective phosphatidylinositol 3-kinase inhibitors to treat hematological malignancies, Drug Discovery Today, 20 (2015) 988-994.

[36] X.B. Tian, H.F. Zhang, T. Heimbach, H.D. He, A. Buchbinder, M. Aghoghovbia, F. Hourcade-Potelleret, Clinical Pharmacokinetic and Pharmacodynamic Overview of Nilotinib, a Selective Tyrosine Kinase Inhibitor, Journal of Clinical Pharmacology, 58 (2018) 1533-1540.

[37] C.T. Durlacher, Z.L. Li, X.W. Chen, Z.X. He, S.F. Zhou, An update on the pharmacokinetics and pharmacodynamics of alisertib, a selective Aurora kinase A inhibitor, Clin Exp Pharmacol P, 43 (2016) 585-601.

[38] W. Zheng, Y. Zhao, Q. Luo, Y. Zhang, K. Wu, F.Y. Wang, Multi-Targeted Anticancer Agents, Current Topics in Medicinal Chemistry, 17 (2017) 3084-3098.

[39] H. Yang, H.R. Lawrence, A. Kazi, H. Gevariya, R. Patel, Y.T. Luo, U. Rix, E. Schonbrunn, N.J. Lawrence, S.M. Sebti, Dual Aurora A and JAK2 kinase blockade effectively suppresses malignant transformation, Oncotarget, 5 (2014) 2947-2961.

[40] S. Howard, V. Berdini, J.A. Boulstridge, M.G. Carr, D.M. Cross, J. Curry, L.A. Devine, T.R. Early, L. Fazal, A.L. Gill, M. Heathcote, S. Maman, J.E. Matthews, R.L. McMenamin, E.F. Navarro, M.A. O'Brien, M. O'Reilly, D.C. Rees, M. Reule, D. Tisi, G. Williams, M. Vinkovic, P.G. Wyatt, Fragment-Based Discovery of the Pyrazol-4-yl Urea (AT9283), a Multitargeted Kinase Inhibitor with Potent Aurora Kinase Activity, Journal of Medicinal Chemistry, 52 (2009) 379-388.

[41] A.K. Samanta, H. Lin, T. Sun, H. Kantarjian, R.B. Arlinghaus, Janus kinase 2: A critical target in chronic myelogenous leukemia, Cancer Research, 66 (2006) 6468-6472.

[42] X. Xue, S.K. Ramakrishnan, K. Weisz, D. Triner, L. Xie, D. Attili, A. Pant, B. Gyorffy, M. Zhan, C. Carter-Su, K.M. Hardiman, T.D. Wang, M.K. Dame, J. Varani, D. Brenner, E.R. Fearon, Y.M. Shah,

Iron Uptake via DMT1 Integrates Cell Cycle with JAK-STAT3 Signaling to Promote Colorectal Tumorigenesis, Cell Metabolism, 24 (2016) 447-461.

[43] G. Goerguen, E. Calabrese, T. Hideshima, J. Ecsedy, G. Perrone, M. Mani, H. Ikeda, G. Bianchi, Y. Hu, D. Cirstea, L. Santo, Y.-T. Tai, S. Nahar, M. Zheng, M. Bandi, R.D. Carrasco, N. Raje, N. Munshi, P. Richardson, K.C. Anderson, Anovel Aurora-A kinase inhibitor MLN8237 induces cytotoxicity and cell-cycle arrest in multiple myeloma, Blood, 115 (2010) 5202-5213.

[44] W. Wang, X. Feng, H.-X. Liu, S.-W. Chen, L. Hui, Synthesis and biological evaluation of 2,4-disubstituted phthalazinones as Aurora kinase inhibitors, Bioorganic & Medicinal Chemistry, 26 (2018) 3217-3226.

[45] Y.-Y. Ke, C.-P. Chang, W.-H. Lin, C.-H. Tsai, I.C. Chiu, W.-P. Wang, P.-C. Wang, P.-Y. Chen, W.-H. Lin, C.-F. Chang, P.-C. Kuo, J.-S. Song, C. Shih, H.-P. Hsieh, Y.-H. Chi, Design and synthesis of BPR1K653 derivatives targeting the back pocket of Aurora kinases for selective isoform inhibition, European Journal of Medicinal Chemistry, 151 (2018) 533-545.

[46] X. Liang, J. Zang, X. Li, S. Tang, M. Huang, M. Geng, C.J. Chou, C. Li, Y. Cao, W. Xu, H. Liu, Y. Zhang, Discovery of Novel Janus Kinase (JAK) and Histone Deacetylase (HDAC) Dual Inhibitors for the Treatment of Hematological Malignancies, Journal of Medicinal Chemistry, 62 (2019) 3898-3923.

[47] L. Shi, Z. Zhong, X. Li, Y. Zhou, Z. Pan, Discovery of an Orally Available Janus Kinase 3 Selective Covalent Inhibitor, Journal of Medicinal Chemistry, 62 (2019) 1054-1066.

[48] J. Bromberg, J.E. Darnell, The role of STATs in transcriptional control and their impact on cellular function, Oncogene, 19 (2000) 2468-2473.

[49] M. Kollareddy, P. Dzubak, D. Zheleva, M. Hajduch, AURORA KINASES: STRUCTURE, FUNCTIONS AND THEIR ASSOCIATION WITH CANCER, Biomedical Papers-Olomouc, 152 (2008) 27-33.

[50] C.C. Mills, E.A. Kolb, V.B. Sampson, Recent Advances of Cell-Cycle Inhibitor Therapies for Pediatric Cancer, Cancer Research, 77 (2017) 6489-6498.

[51] W. Petersen, J. Liu, L. Yuan, H. Zhang, M. Schneiderjan, Y.-J. Cho, T.J. MacDonald, Dasatinib suppression of medulloblastoma survival and migration is markedly enhanced by combining treatment with the aurora kinase inhibitor AT9283, Cancer Letters, 354 (2014) 68-76.

[52] Y. Wang, C. Peng, G. Wang, Z. Xu, Y. Luo, J. Wang, W. Zhu, Exploring binding mechanisms of VEGFR2 with three drugs lenvatinib, sorafenib, and sunitinib by molecular dynamics simulation and

free energy calculation, Chem Biol Drug Des, 93 (2019) 934-948.

[53] M.A. Kashem, R.M. Nelson, J.D. Yingling, S.S. Pullen, A.S. Prokopowicz, III, J.W. Jones, J.P. Wolak, G.R. Rogers, M.M. Morelock, R.J. Snow, C.A. Homon, S. Jakes, Three mechanistically distinct kinase assays compared: Measurement of intrinsic ATPase activity identified the most comprehensive set of ITK inhibitors, Journal of Biomolecular Screening, 12 (2007) 70-83.

[54] O. Trott, A.J. Olson, AutoDock Vina: Improving the speed and accuracy of docking with a new scoring function, efficient optimization, and multithreading, Journal of Computational Chemistry, 31 (2010) 455-461.

[55] S. Howard, V. Berdini, J.A. Boulstridge, M.G. Carr, D.M. Cross, J. Curry, L.A. Devine, T.R. Early, L. Fazal, A.L. Gill, M. Heathcote, S. Maman, J.E. Matthews, R.L. McMenamin, E.F. Navarro, M.A. O'Brien, M. O'Reilly, D.C. Rees, M. Reule, D. Tisi, G. Williams, M. Vinković, P.G. Wyatt, Fragment-Based Discovery of the Pyrazol-4-yl Urea (AT9283), a Multitargeted Kinase Inhibitor with Potent Aurora Kinase Activity, Journal of Medicinal Chemistry, 52 (2009) 379-388.

[56] S. Jaime-Figueroa, J. De Vicente, J. Hermann, A. Jahangir, S. Jin, A. Kuglstatter, S.M. Lynch, J. Menke, L. Niu, V. Patel, A. Shao, M. Soth, M.D. Vu, C. Yee, Discovery of a series of novel 5H-pyrrolo[2,3-b]pyrazine-2-phenyl ethers, as potent JAK3 kinase inhibitors, Bioorganic & Medicinal Chemistry Letters, 23 (2013) 2522-2526.

[57] J.M. Elkins, S. Santaguida, A. Musacchio, S. Knapp, Crystal Structure of Human Aurora B in Complex with INCENP and VX-680, Journal of Medicinal Chemistry, 55 (2012) 7841-7848.

[58] G.M. Morris, R. Huey, W. Lindstrom, M.F. Sanner, R.K. Belew, D.S. Goodsell, A.J. Olson, AutoDock4 and AutoDockTools4: Automated docking with selective receptor flexibility, Journal of computational chemistry, 30 (2009) 2785-2791.

[59] N.M. O'Boyle, M. Banck, C.A. James, C. Morley, T. Vandermeersch, G.R. Hutchison, Open Babel: An open chemical toolbox, Journal of cheminformatics, 3 (2011) 33.

[60] M.S. Marlow, J. Dogan, K.K. Frederick, K.G. Valentine, A.J. Wand, The role of conformational entropy in molecular recognition by calmodulin, Nature chemical biology, 6 (2010) 352-358.

[61] J.A. Maier, C. Martinez, K. Kasavajhala, L. Wickstrom, K.E. Hauser, C. Simmerling, ff14SB: Improving the Accuracy of Protein Side Chain and Backbone Parameters from ff99SB, Journal of Chemical Theory and Computation, 11 (2015) 3696-3713.

[62] J. Wang, R.M. Wolf, J.W. Caldwell, P.A. Kollman, D.A. Case, Development and testing of a

general amber force field, Journal of computational chemistry, 25 (2004) 1157-1174.

[63] W.L. Jorgensen, J. Chandrasekhar, J.D. Madura, R.W. Impey, M.L. Klein, Comparison of simple potential functions for simulating liquid water, The Journal of chemical physics, 79 (1983) 926.

[64] J.-P. Ryckaert, G. Ciccotti, H.J. Berendsen, Numerical integration of the cartesian equations of motion of a system with constraints: molecular dynamics of< i> n</i>-alkanes, Journal of Computational Physics, 23 (1977) 327-341.

[65] T. Darden, D. York, L. Pedersen, Particle mesh Ewald: An N· log (N) method for Ewald sums in large systems, The Journal of chemical physics, 98 (1993) 10089.

[66] A. Onufriev, D. Bashford, D.A. Case, Exploring protein native states and large- scale conformational changes with a modified generalized born model, Proteins: Structure, Function, and Bioinformatics, 55 (2004) 383-394.

[67] M.F. Sanner, A.J. Olson, J.-C. Spehner, Reduced surface: An efficient way to compute molecular surfaces, Biopolymers, 38 (1996) 305-320.

Highlights

- Compound **10e** is a multi-targeted inhibitor with with IC_{50} of 0.166 μM (JAK2), 0.057 μM (JAK3), 0.939 μM (Aurora A) and 0.583 μM (Aurora B), respectively.
- Compound **10e** exhibited moderate anti-proliferative activities against K562 (IC_{50}=6.726μM).
- Compound **10e** down-regulates the phosphorylation of STAT3, STAT5, Aurora A and Aurora B in a dose-dependent manner in K562 and HCT116 cells.
- Compound **10e** inhibited the proliferation of cells by inducing cell cycle arrest in G2 phase.
- Compound **10e** could maintain quite similar binding mode of JAK 2/3 and Aurora A/B kinases as multi-target kinase inhibitor (AT9832).

Declaration of interests

☒ The authors declare that they have no known competing financial interests or personal relationships that could have appeared to influence the work reported in this paper.

☐The authors declare the following financial interests/personal relationships which may be considered as potential competing interests:

You-Guang Zheng, Jin-An Wang, Long Meng, Xin Pei, Ling Zhang, Lin An, Cheng-Lin Li, Ying-Long Miao.